

Electronic Supplementary Information

**Controlled Synthesis of High Quality Scandium-based
Nanocrystals as Promising Recyclable Catalysts for
Silylcyanation Reaction**

Boyan Yu,^{ab} Erjun Hao,^c Shaoming Fang,^d Zhengqing Liu,^{ab} Yongwei Wang,^d
Zhenzhen Lv,^a Na Li,^{ab} Xinyu Zhang,^{ab} Lei Shi^{*a} and Yaping Du^{*ab}

a. Frontier Institute of Science and Technology jointly with College of Science, State Key Laboratory for Strength and Vibration of Mechanical Structures, Xi'an Jiaotong University, Xi'an 710049, P.R. China.

b. State Key Laboratory of Chemo/Biosensing and Chemometrics, Hunan University, Changsha 410082, P.R. China. E-mail: ypdu2013@mail.xjtu.edu.cn

c. Key Laboratory of Green Chemical Media and Reactions, Ministry of Education, Collaborative Innovation Center of Henan Province for Green Manufacturing of Fine Chemicals, School of Chemistry and Chemical Engineering, Henan Normal University, Xinxiang, Henan 453007, P.R. China.

d. State Laboratory of Surface and Interface Science and Technology, Zhengzhou University of Light Industry, Zhengzhou 450002, P.R. China.

Experimental

Chemicals

Oleylamine (OM, 70%) and oleic acid (OA, 90%) were purchased from Aldrich and used without further purification. The scandium (III) oxide (Sc_2O_3 , 99.9%), sodium trifluoroacetate (CF_3COONa , 99.9%), potassium trifluoroacetate (CF_3COOK , 99.9%) were purchased from Alfa Aesar and used as received. The trifluoroacetic acid (CF_3COOH , >99.0%) was obtained from TCI. Aromatic aldehydes and cyanotrimethylsilane (TMSCN) were obtained from Alfa Aesar and used without further purification. Absolute ethanol, methanol, cyclohexane and acetonitrile were analytical reagent grade, and acetonitrile was distilled before use.

Synthesis of $\text{Sc}(\text{CF}_3\text{COO})_3$

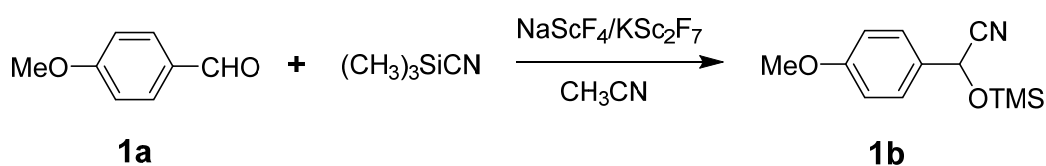
3 g of Sc_2O_3 was added into 10 mL of DI water in a flask (50 mL) at room temperature. 6 mL of CF_3COOH was added into the slurry with magnetic stirring and the mixture was heated to 80 °C. Then, around every 6 hours later, 1 mL of CF_3COOH was added, till the solution was totally transparent. After filtration, the mixture was transferred into a crucible and dried in air at 100 °C overnight.

Synthesis of NaScF_4 and KSc_2F_7 nanocrystals

The synthesis of NaScF_4 and KSc_2F_7 nanocrystals was established *via* the modified thermal decomposition method. A given amount of CF_3COONa (or CF_3COOK) and $\text{Sc}(\text{CF}_3\text{COO})_3$ (0.3 mmol) were added into 10 mmol of OA/OM (the ratio of OA:OM was changed from 1:1 to 4:1) in a three-necked flask (50 mL). The mixture was heated to 120 °C to remove dissolved gas, water and organic impurities with low boiling points, with vigorous magnetic stirring under vacuum for 30 min, and thus forming a transparent liquid. Then the mixture was heated to a certain temperature within the range of 270-330 °C rapidly, and kept at the temperature for 30-120 min under a N_2 atmosphere. After the reaction was completed and cooled to room temperature, a proper amount of ethanol was added into the mixture. The consequent mixture was separated by centrifugation at 9000 r/min and the products were collected. The products were washed ~3 times with the mixture of ethanol and a small amount of cyclohexane, and dried in a vacuum drying oven at 60 °C overnight.

General experimental of catalysis

All manipulations with air-sensitive reagents were carried out under a dry nitrogen atmosphere. Commercial reagents were used as received without further purification unless otherwise stated. All solvents used were dried using standard, published methods and were distilled before use. NaScF_4 and KSc_2F_7 nanocrystals were used after surface modification.



As for the synthesis of **1b**, to a suspension of $\text{NaScF}_4/\text{KSc}_2\text{F}_7$ (3.6 mg/6.6 mg,

0.025 mmol) in freshly distilled acetonitrile (1 mL) was added cyanotrimethylsilane (TMSCN) (131.2 μL , 1.2 mmol) and Anisic aldehyde (59.0 μL , 0.5 mmol). The reaction was stirred at room temperature until the reaction was complete, as indicated by $^1\text{H-NMR}$ analysis. The reaction mixture was centrifuged, and the upper supernatant was evaporated to get the product of **1b** (the conversion ratio is ~99%).

Instrumentation

Powder X-ray diffraction (XRD) patterns were recorded on D/MAX-RB SMARTLAB(3) diffractometer (Rigaku, Japan) at the scanning rate of 10°min^{-1} with a slit of $(1/2)^\circ$, using Cu- $K\alpha$ radiation ($\lambda = 1.5418 \text{ \AA}$), and the operating voltage was 40 kV with operating current of 30 mA. X-ray photoelectron spectroscopy (XPS) spectra were acquired with K-Alpha+ X-ray photoelectron spectrometer (Thermo Fisher, the USA). Transmission electron microscopy (TEM) images were acquired with a Hitachi HT-7700 transmission electron microscope (Japan) operated at 100 kV. High-resolution TEM (HRTEM) micrographs were obtained with a Philips Tecnai F20 FEG-TEM (The USA) operated at 200 kV. Samples for TEM analysis were prepared on amorphous carbon coated copper grids by drying a drop of dispersion liquid of nanocrystals in cyclohexane. Infrared spectra were recorded on a Nicolet 6700 Fourier transform infrared (FT-IR) spectrometer (Thermo Fisher, the USA). Thermogravimetry (TG) curves were recorded on TGA 4000 thermogravimetric analyzer (PerkinElmer, the USA). Nuclear magnetic resonance (NMR) spectra were measured on a Bruker Avance-400 spectrometer (the USA) and chemical shifts (δ) were reported in parts per million (ppm). $^1\text{H-NMR}$ spectra were recorded at 400 MHz in NMR solvents and referenced internally to corresponding solvent resonance, and $^{13}\text{C-NMR}$ spectra were recorded at 100 MHz and referenced to corresponding solvent resonance. The specific surface areas and pore sizes were estimated with Autosorb-iQ-C automated physisorption and chemisorption analyzer (Quantachrome, the USA) and the assistance of Brunauer-Emmett-Teller (BET) method, by nitrogen adsorption at 77 K. Before the adsorption desorption measurements, the samples (after thermal treatment) were degassed at 453 K for 10 h. Atomic emission spectra (AES) data were tested on Plasma 1000 inductively coupled plasma atomic emission spectrometer (ICP-AES, NCS, China).

Controlled synthesis of high quality NaScF₄ nanocrystals

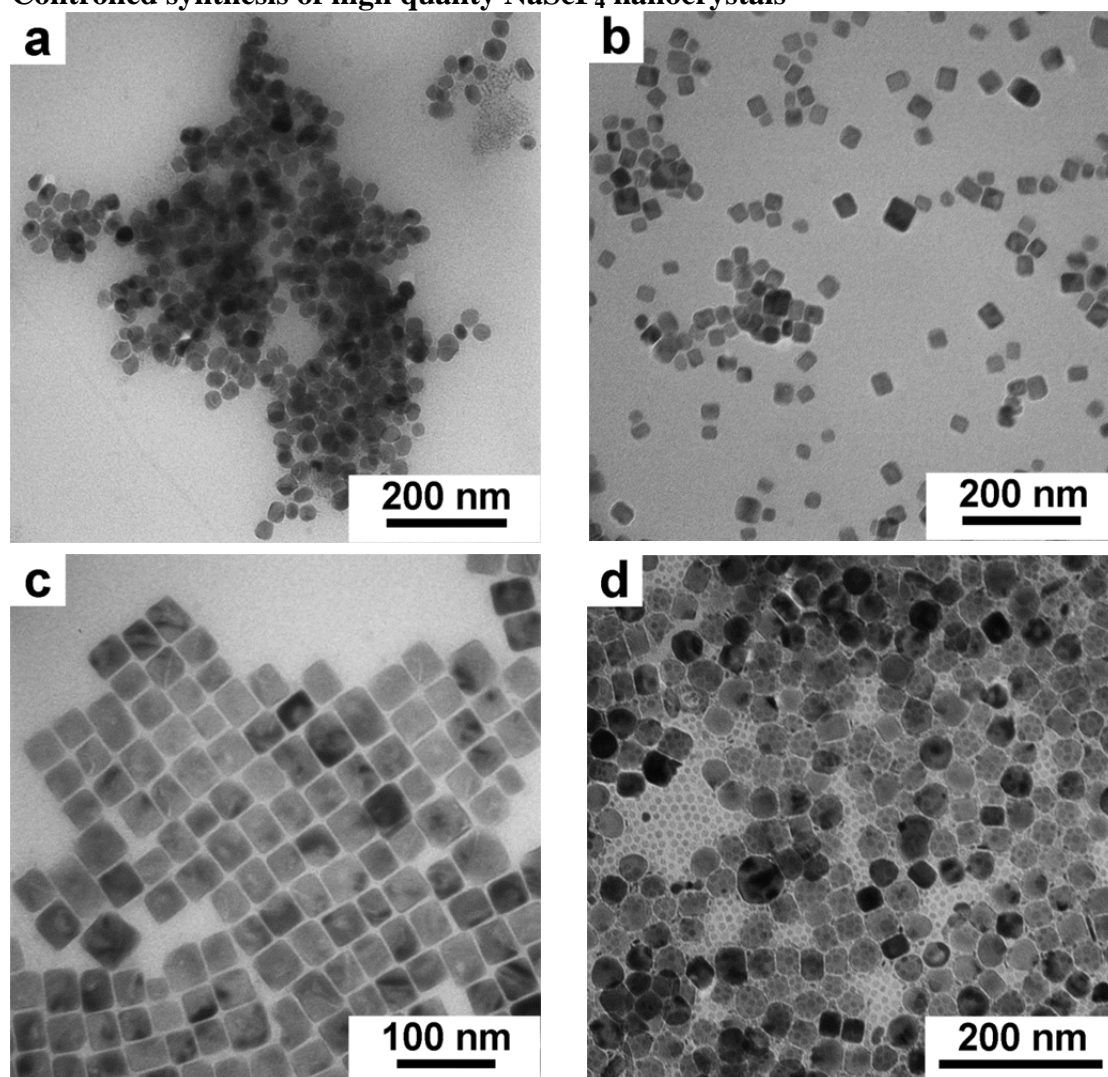


Fig. S1 TEM images of NaScF₄ nanocrystals obtained under different solvent ratio: (a) OA:OM = 1:1; (b) OA:OM = 2:1; (c) OA:OM = 3:1; (d) OA:OM = 4:1. The reactions are conducted of 0.3 mmol CF₃COONa and 0.3 mmol Sc(CF₃COO)₃ in the solvent of OA and OM (10 mmol in total) at 310 °C for 1 h.

The ratio of OA and OM. With the increase of the proportion of OA, from OA:OM = 1:1 to 4:1, the morphology became uniform gradually (**Fig. S1a, b and c**) and then disordered (**Fig. S1d**). It can be easily noticed that the optimum ratio of OA and OM for synthesis is 3:1.

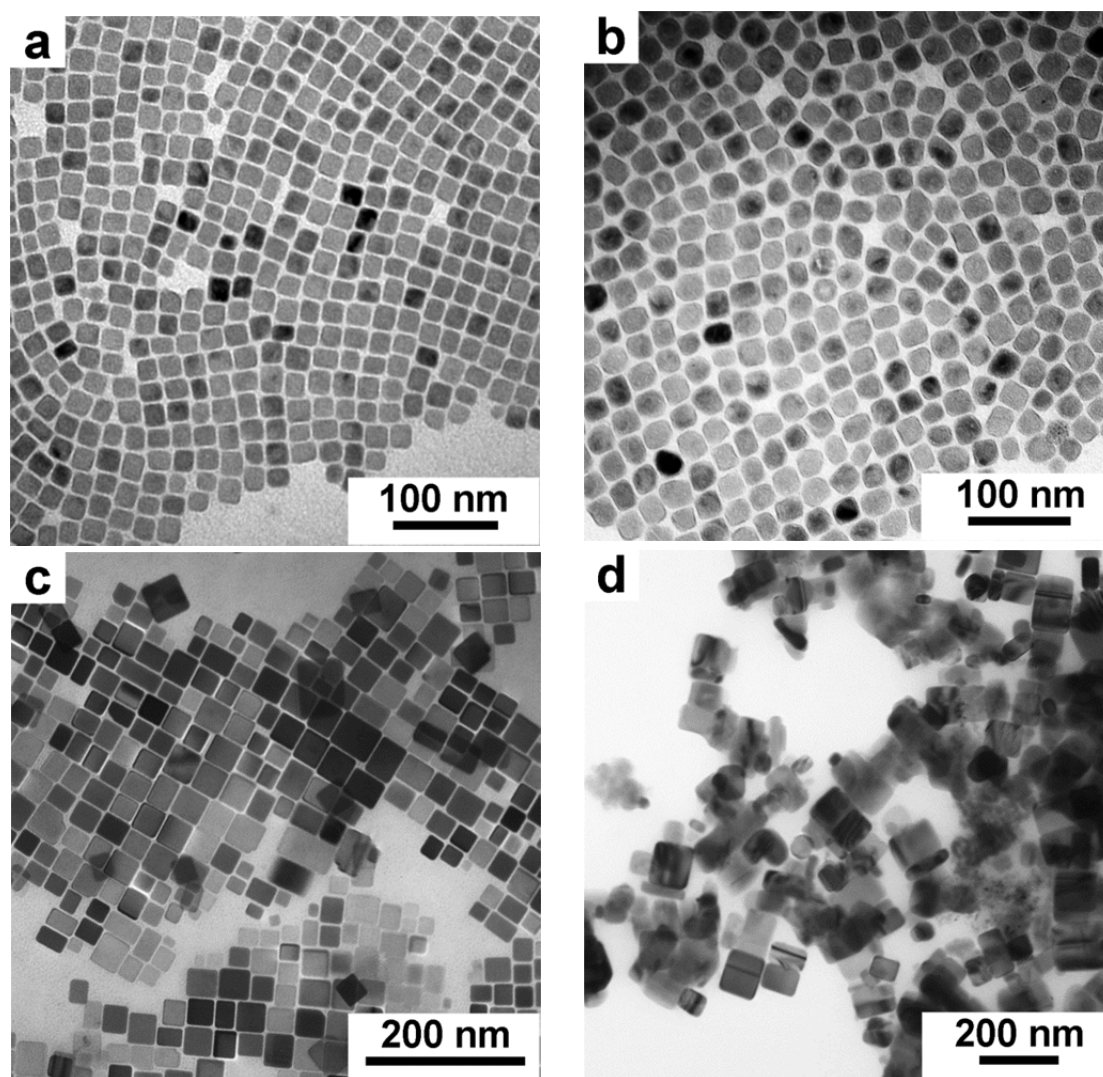


Fig. S2 TEM images of NaScF_4 nanocrystals obtained at different reaction temperature: (a) 270 °C; (b) 290 °C; (c) 310 °C; (d) 330 °C; The reactions are conducted of 0.3 mmol CF_3COONa and 0.3 mmol $\text{Sc}(\text{CF}_3\text{COO})_3$ in the solvent of OA:OM = 3:1 (10 mmol in total) for 1 h.

Reaction temperature. As showed in **Fig. S2**, nanocrystals obtained at lower temperatures were with smaller sizes (**Fig. S2a** and **b**). When synthesized at 310 °C, the nanocrystals had uniform morphologies and larger sizes (**Fig. S2c**). Further elevating the temperature, the nanocrystals became non-uniform (**Fig. S2d**). Therefore, the temperature which is not higher than 310 °C is the optimum temperature for synthesis.

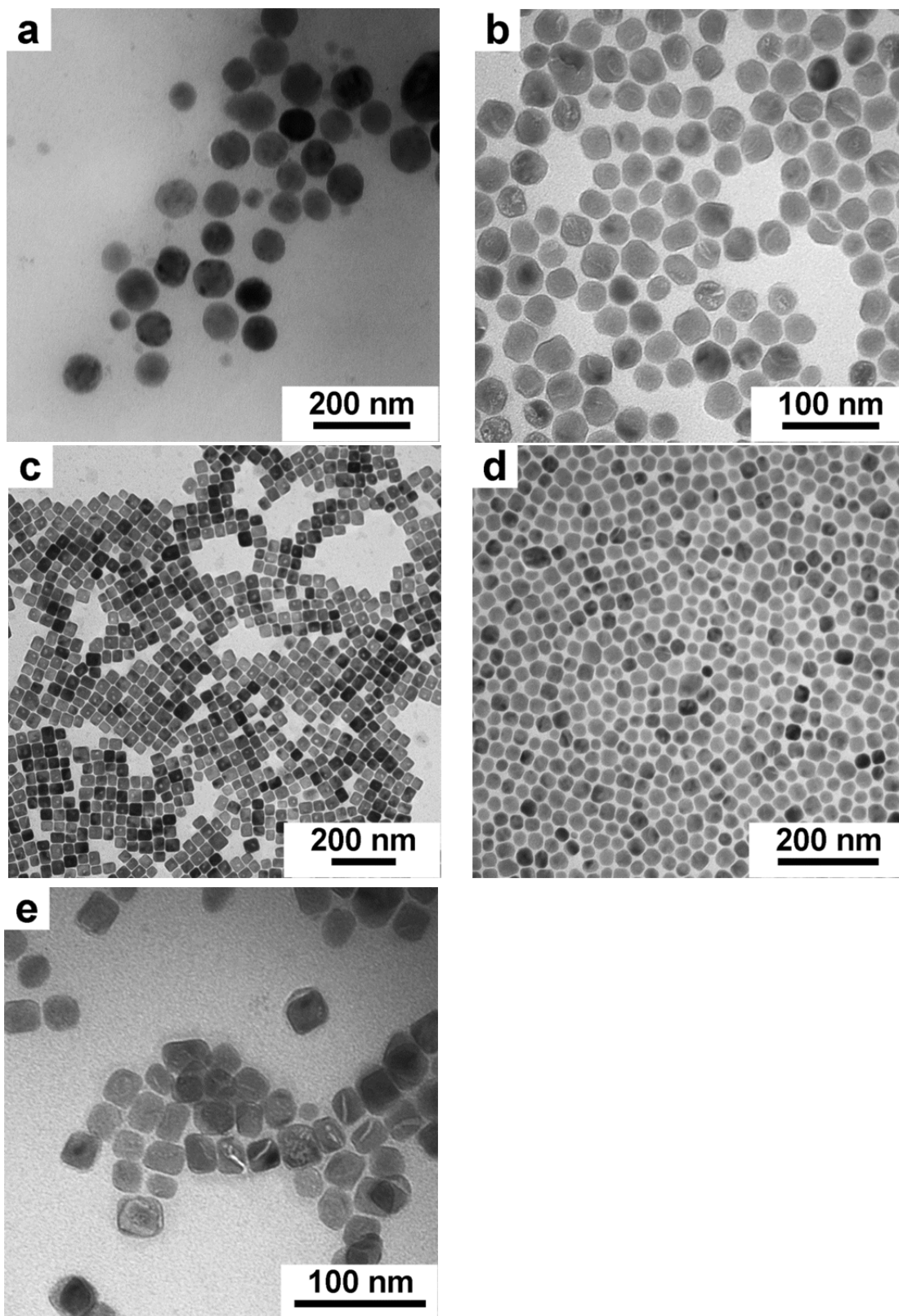


Fig. S3 TEM images of NaScF₄ nanocrystals obtained at different reaction time: (a) 0 min; (b) 30 min; (c) 60 min; (d) 90 min; (e) 120 min. The reactions are conducted of 0.3 mmol CF₃COONa and 0.3 mmol Sc(CF₃COO)₃ in the solvent of OA:OM = 3:1 (10 mmol in total) at 310 °C.

Reaction time. TEM images of nanocrystals obtained at different reaction time demonstrate the growing process of NaScF₄ nanocrystals, as shown in **Fig. S3**. With

the synthesis continued from the beginning to 60 min (**Fig. S3a to c**), the square-like nanocrystals formed gradually. Further prolonging the reaction time, the nanocrystals were getting non-uniform (**Fig. S3d**) and even aggregation (**Fig. S3e**). Therefore, 60 min is the optimum reaction time for synthesis.

Controlled synthesis of KSc_2F_7 nanocrystals

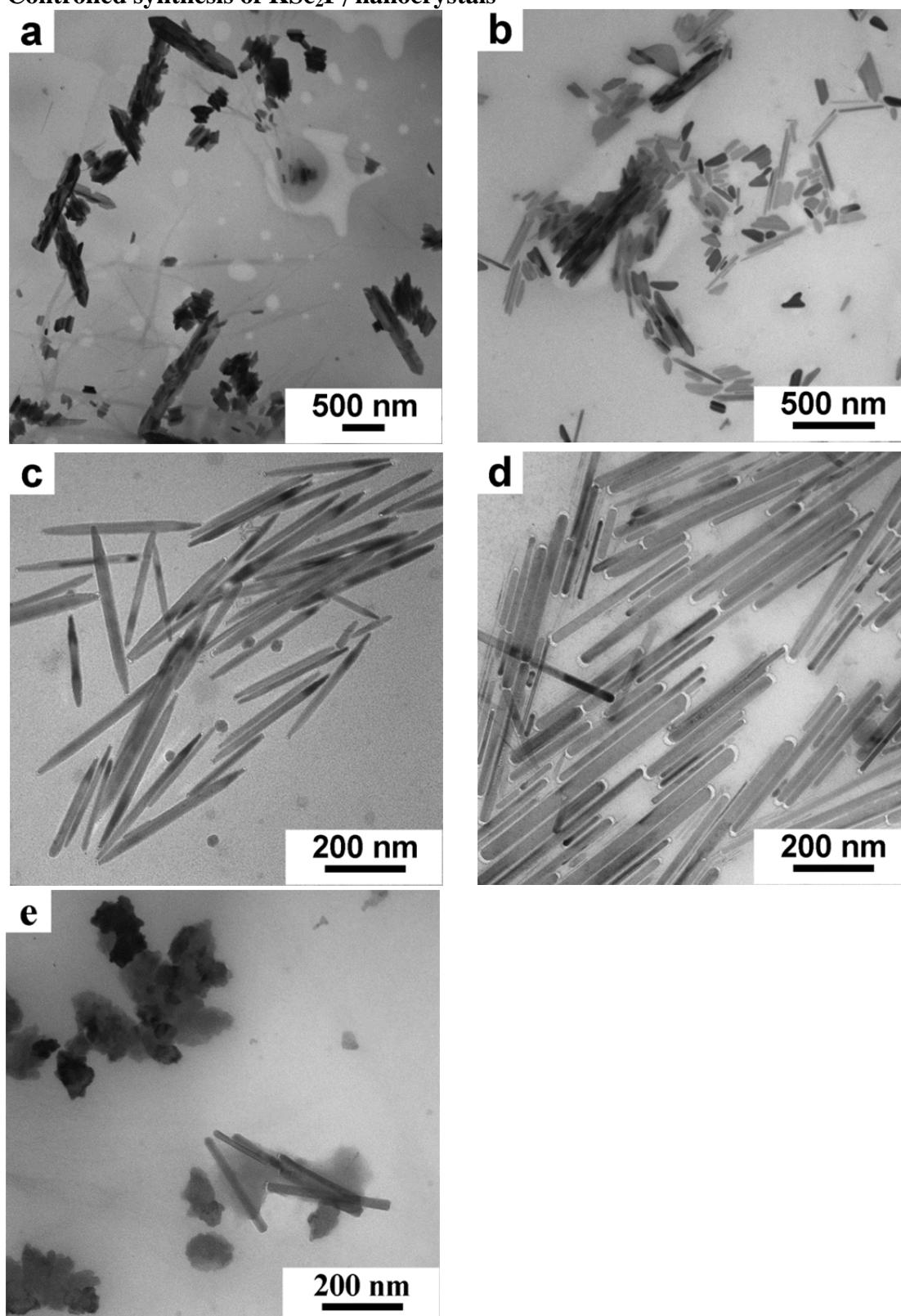


Fig. S4 TEM images of KSc_2F_7 nanocrystals obtained under different solvent ratio: (a) OA = 10 mmol; (b) OA:OM = 1:1; (c) OA:OM = 2:1; (d) OA:OM = 3:1; (e) OA:OM = 4:1. The reactions are conducted of 0.3 mmol CF_3COOK and 0.3 mmol $\text{Sc}(\text{CF}_3\text{COO})_3$, in 10 mmol OA and OM in total, at 310 °C for 1 h.

The ratio of OA and OM. The nanocrystals synthesized in pure OA were messy (**Fig. S4a**). With the increase of the proportion of OA from 1:1 to 3:1, the size and morphology was getting monodisperse (**Fig. S4b, c and d**). Further increasing the amount of OA, the as-obtained products were severely aggregated and non-shaped (**Fig. S4e**). Hence, the optimum ratio of OA and OM for synthesis is 3:1.

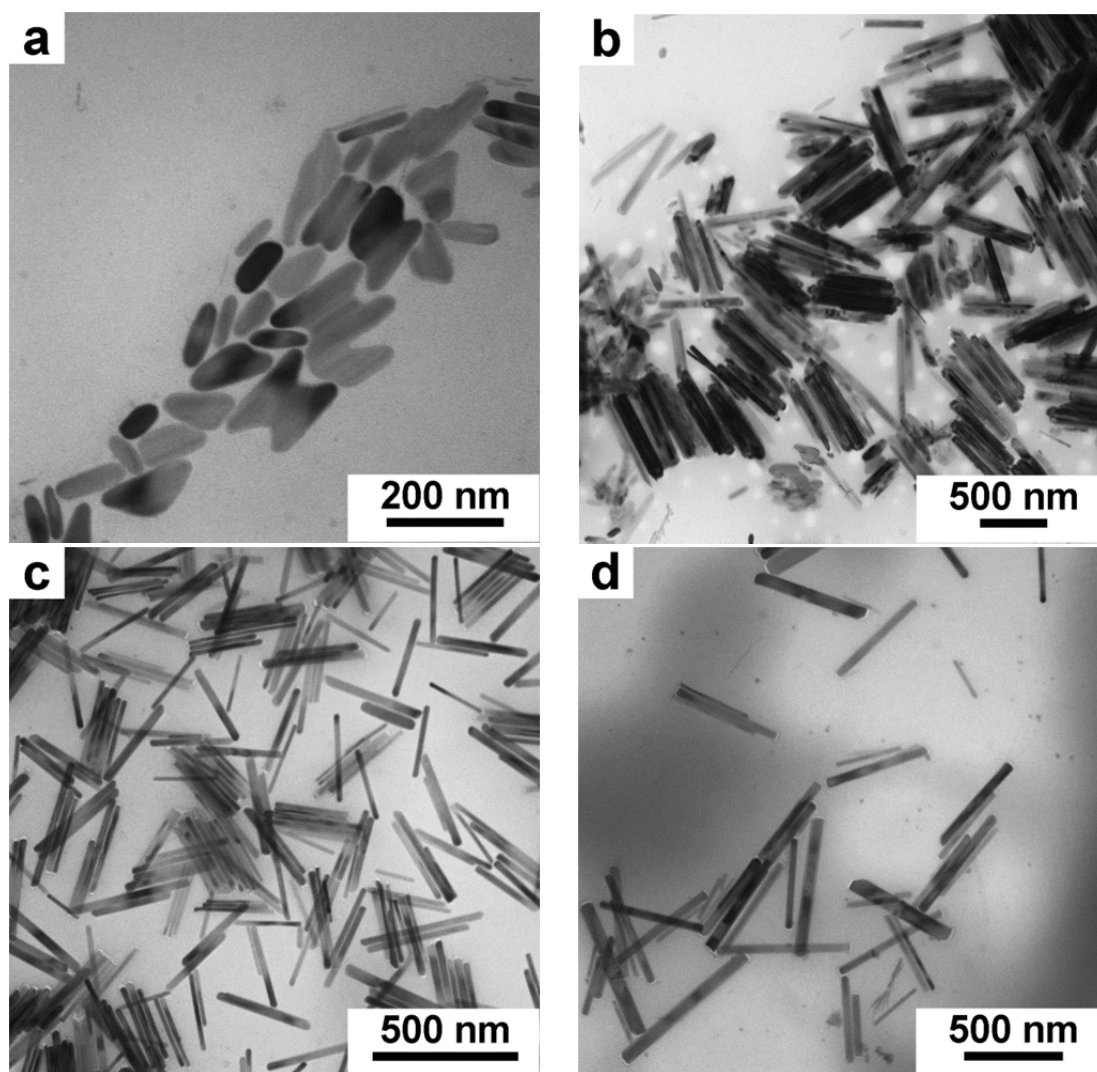


Fig. S5 TEM images of KSc_2F_7 nanorods obtained at different reaction temperature: (a) 270 °C; (b) 290 °C; (c) 310 °C; (d) 330 °C; The reactions are conducted of 0.3 mmol CF_3COOK and 0.3 mmol $\text{Sc}(\text{CF}_3\text{COO})_3$ in the solvent of OA:OM = 3:1 (10 mmol in total) for 1 h.

Reaction temperature. As showed in **Fig. S5**, when the temperatures were low, nanocrystals were non-uniform in sizes and morphologies (**Fig. S5a and b**). Nanocrystals obtained at 310 °C had relatively uniform morphologies and sizes (**Fig. S5c**), which was the optimum temperature for synthesis. Further increasing the reaction temperature will result in nonuniform nanocrystals with low yields (**Fig. S5d**).

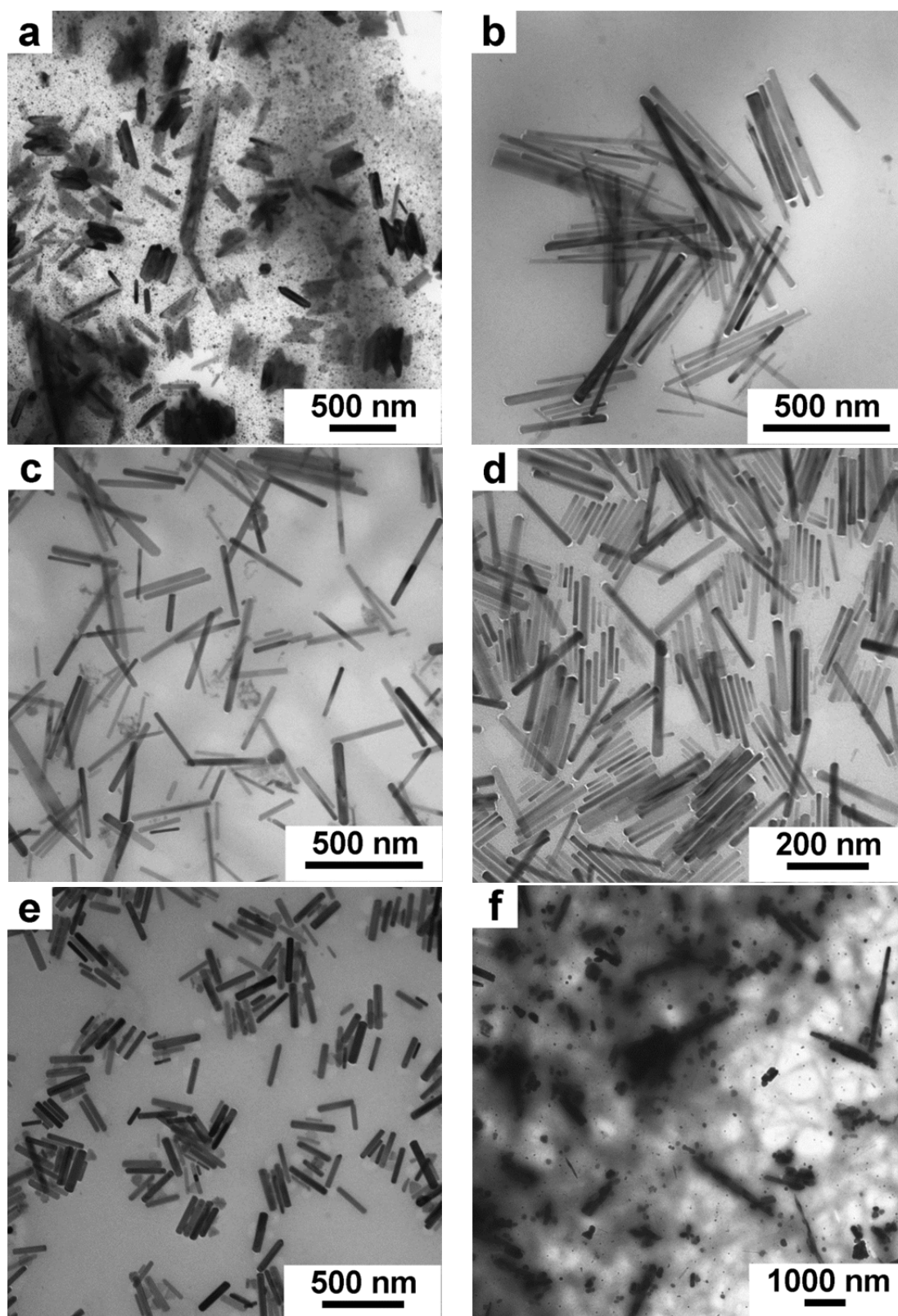


Fig. S6 TEM images of KSc_2F_7 nanocrystals obtained at different reaction time: (a) 0 min; (b) 30 min; (c) 60 min; (d) 90 min; (e) 120 min; (f) 150 min. The reactions are conducted of 0.3 mmol CF_3COOK and 0.3 mmol $\text{Sc}(\text{CF}_3\text{COO})_3$ in the solvent of OA:OM = 3:1 (10 mmol in total) at 310 °C.

Reaction time. TEM images of nanocrystals obtained at different reaction time demonstrate the growing process of KSc_2F_7 nanocrystals, as shown in **Fig. S6**. From the beginning to 60 min (**Fig. S6a to c**), nanocrystals became uniform gradually. With the reaction continuing, the nano-products were non-uniform (**Fig. S6d**) and accompanied with the aggregations (**Fig. S6e**), even occurred the Ostwald ripening process (**Fig. S6f**). Therefore, the optimum reaction time is 60 min for the synthesis.

XPS spectra of NaScF_4 nanocrystals

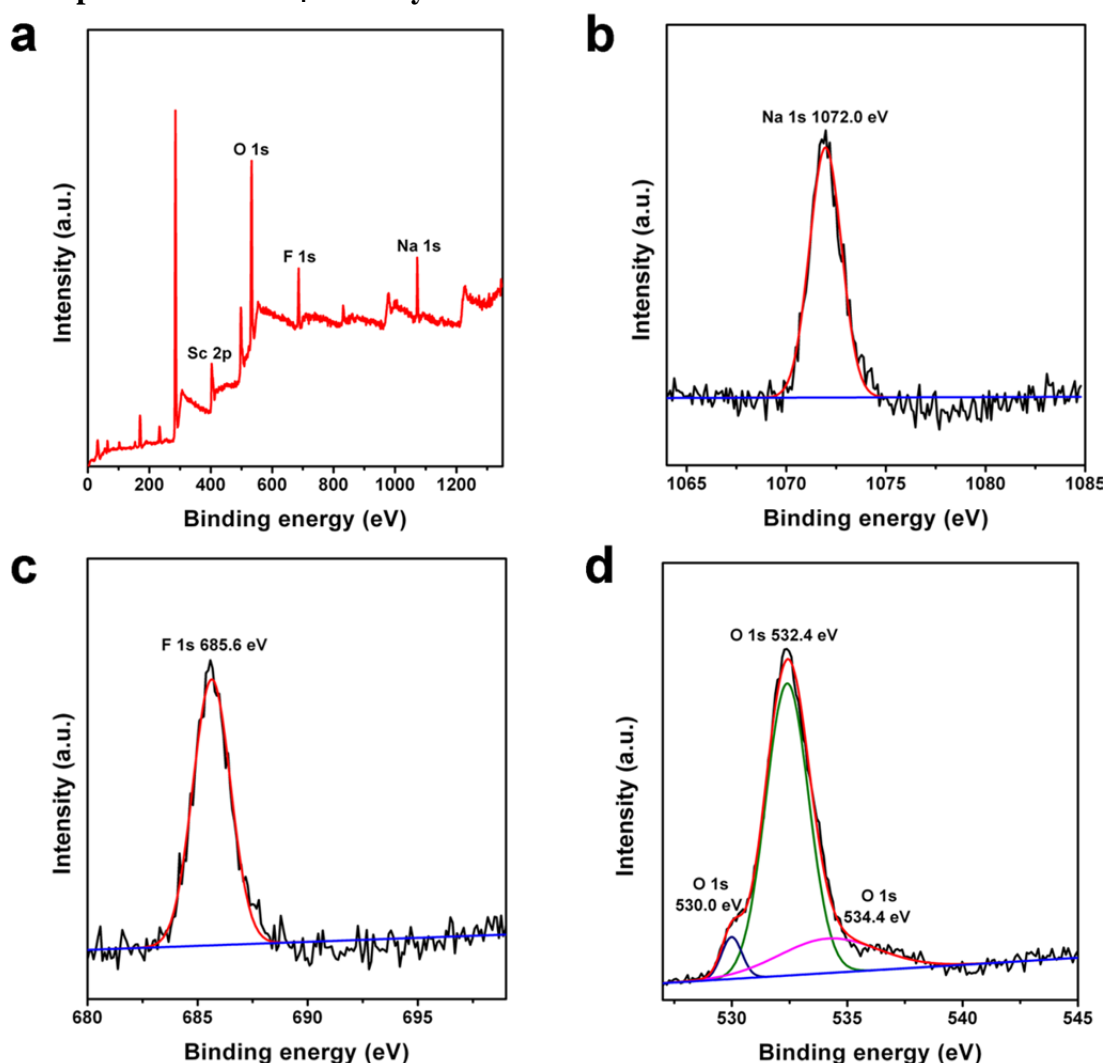


Fig. S7 XPS spectra of NaScF_4 nanocrystals: (a) survey, (b) Na 1s, (c) F 1s, (d) O 1s.

The binding energy of Na, Sc and F element are noted in the XPS survey spectrum (**Fig. S7a**). In **Fig. S7b**, the peak located at 1072.0 eV attributed to the Na 1s spin orbital. And the peak located at 685.6 eV (**Fig. S7c**) represents the F 1s spin orbital. The peak located at 530.0 eV (**Fig. S7f**) indicates that a very small part of the sample is oxidized, and peaks located at 532.4 eV and 534.4 eV are the O 1s signals of adsorbed oxygen. XPS signals of the sample indicate that the sample is nearly pure NaScF_4 , with a little oxidation.

Size distribution histogram of NaScF₄ nanocrystals.

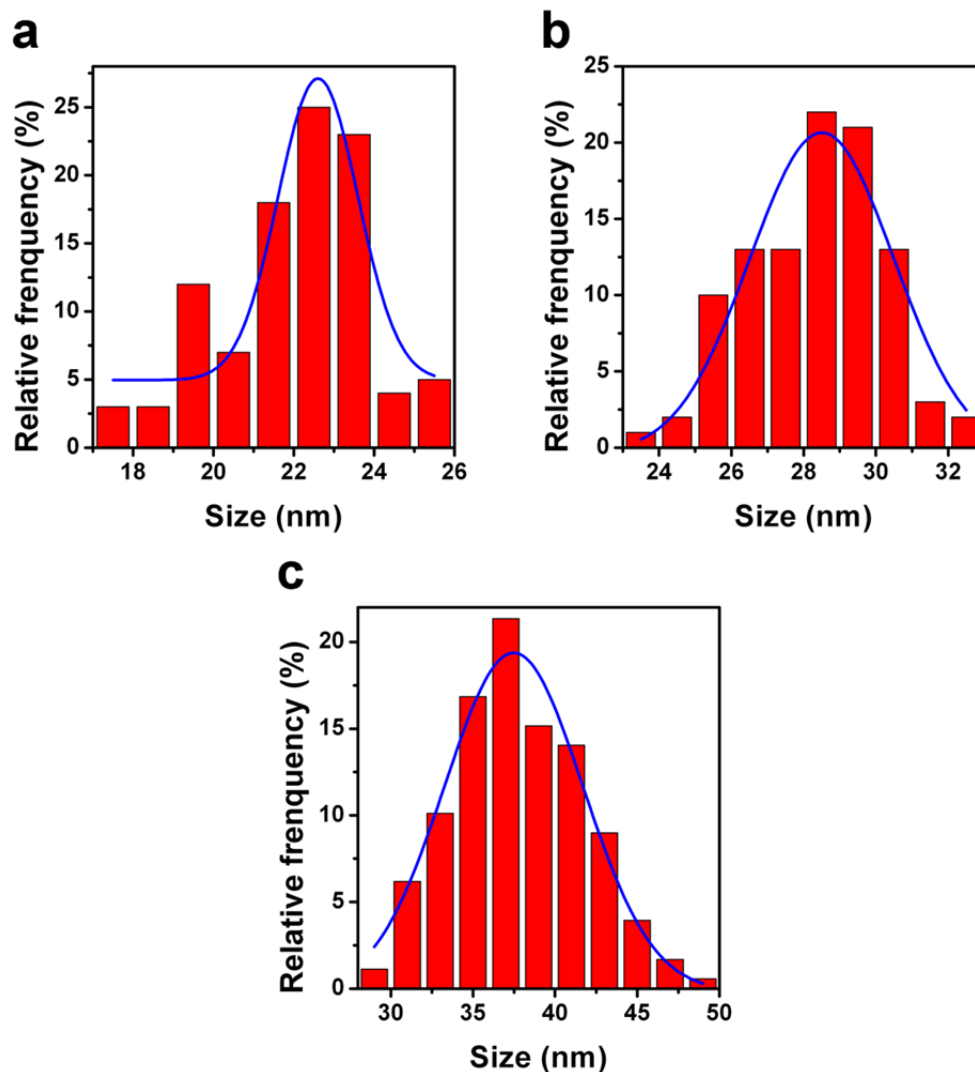


Fig. S8 Size distribution histograms of NaScF₄ nanocrystals obtained at different reaction temperature: (a) 270 °C, (b) 290 °C and (c) 310 °C; As the histograms showed, the size is ~22 nm, ~29 nm and ~38 nm for the nanocrystals synthesized at 270 °C, 290 °C and 310 °C, respectively. The reactions are conducted of 0.3 mmol CF₃COONa and 0.3 mmol Sc(CF₃COO)₃, in the solvent of OA:OM = 3:1 (10 mmol in total) for 1 h.

XRD pattern and XPS spectra of KSc_2F_7 nanocrystals

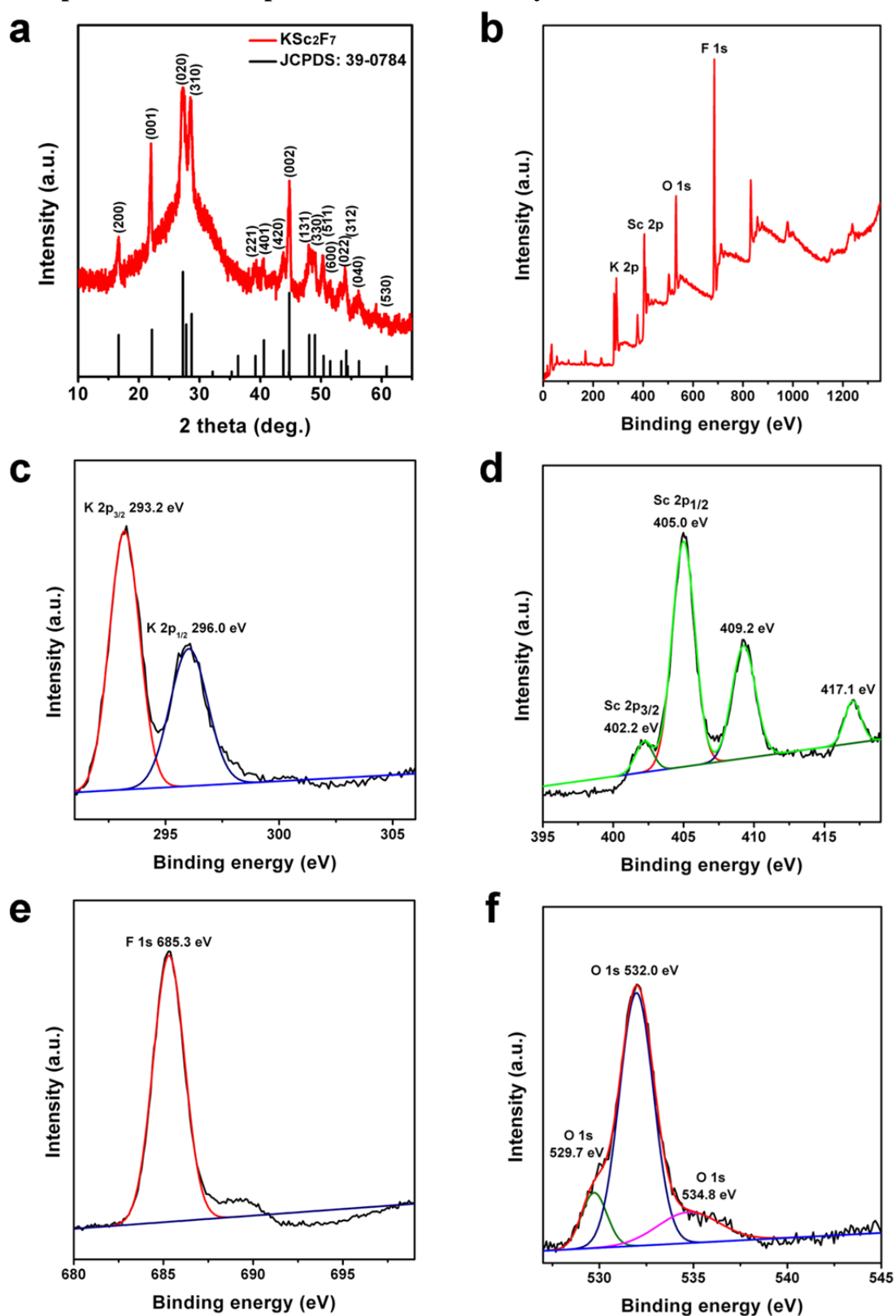


Fig. S9 (a) XRD pattern of KSc_2F_7 nanocrystals; (b-f) XPS spectra of KSc_2F_7 nanocrystals: (b) survey, (c) K 2p, (d) Sc 2p, (e) F 1s, (f) O 1s.

X-ray diffraction (XRD) pattern of NaScF_4 nanocrystals (**Fig. S9a**) shows that all

diffraction peaks can be well matched with the orthorhombic phase KSc_2F_7 (JCPDS No. 34-0394) with calculated $a=10.643 \text{ \AA}$, $b=6.540 \text{ \AA}$, $c=4.030 \text{ \AA}$. The binding energy of K, Sc and F element is noted in the XPS survey spectrum (**Fig. S9b**). In **Fig. S9c**, the peaks located at 293.2 eV and 296.0 eV represent the K $2p_{3/2}$ and K $2p_{1/2}$ spin orbital, respectively. XPS spectrum of Sc in KSc_2F_7 (**Fig. S9d**) includes four peaks because of the appearance of satellite peaks, which arising from the high Sc content of the sample, and the usage of electron floodgun (Ref: A. D. Hamer, D. G. Tisley and R. A. Walton, *J. Inorg. Nucl. Chem.*, 1974, **36**, 1771.). The state of Sc is still inferred from Sc $2p_{3/2}$ and Sc $2p_{1/2}$ signals of the sample, which are 402.2 eV and 405.0 eV and confirm the Sc in the sample is Sc^{3+} state. The peak located at 685.3 eV (**Fig. S9e**) represents the F 1s spin orbital. The peak located at 529.7 eV (**Fig. S9f**) indicates that there is a very small part of the sample is oxidized, and peaks located at 532.0 eV and 534.8 eV are the O 1s signals of adsorbed oxygen. XPS signals of the sample indicate that the sample is nearly pure KSc_2F_7 , with a little oxidation. (Ref: J. F. Moulder, W. F. Stickle, P. E. Sobol and K. D. Bomben, *Handbook of X-ray Photoelectron Spectroscopy*, Perkin-Elmer Corporation: Eden Prairie, MN, 1992.).

Size distribution histograms of KSc_2F_7 nanocrystals

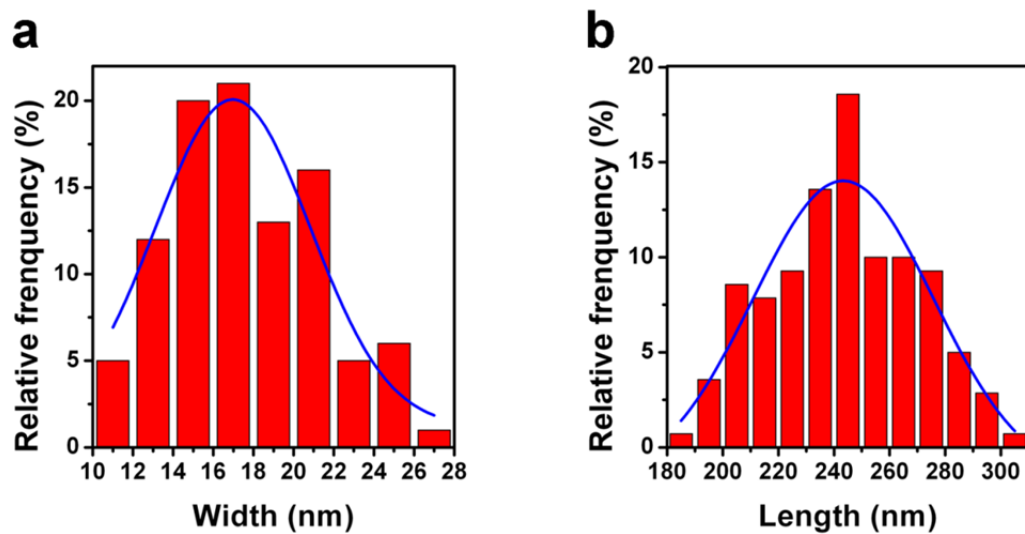


Fig. S10 Size distribution histograms of KSc_2F_7 nanocrystals: (a) width distribution histogram and (b) length distribution histogram.

As shown in above, the average size of KSc_2F_7 nanocrystals is of ~ 17 nm in width and ~ 240 nm in length.

Surface modification of NaScF₄ and KSc₂F₇ nanocrystals

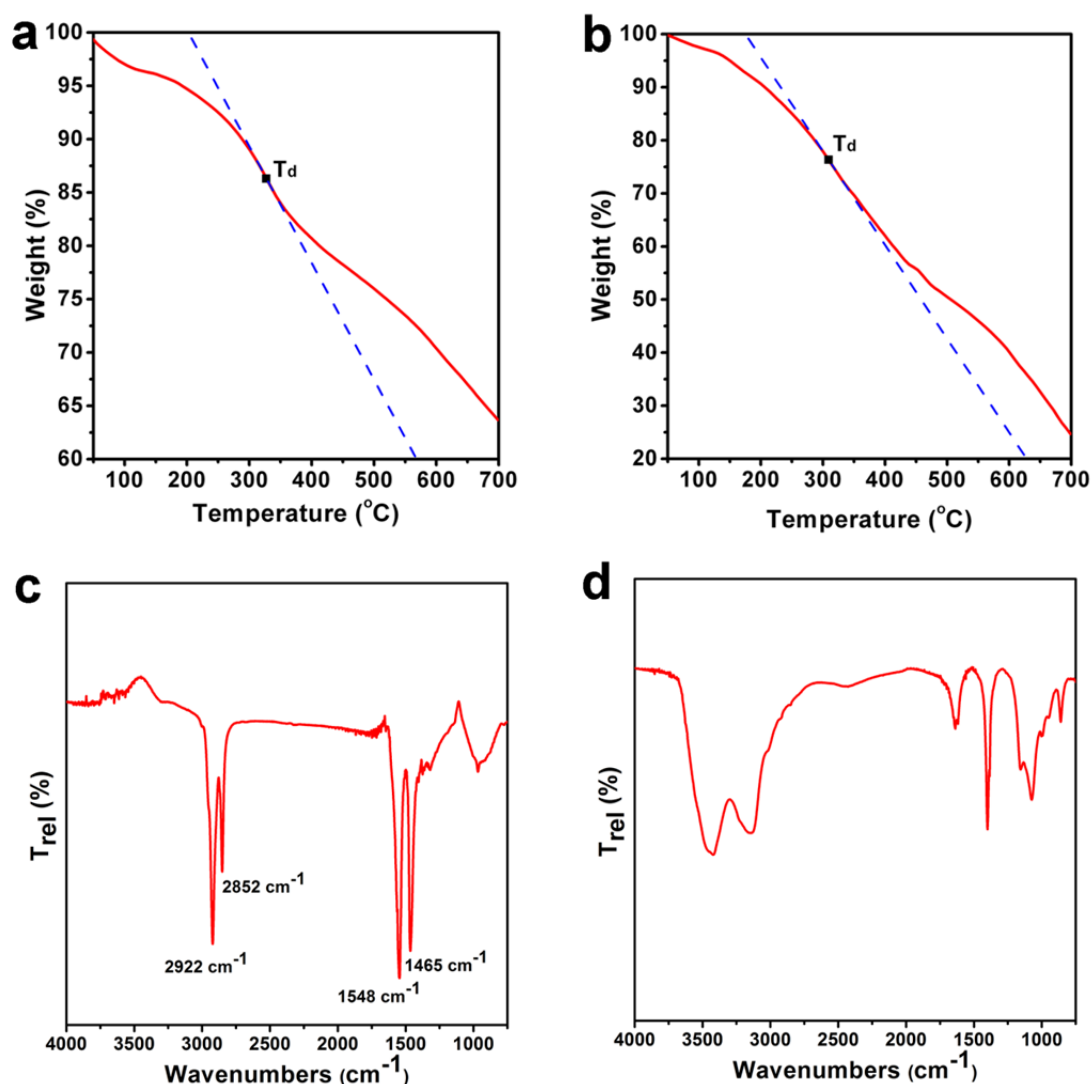


Fig. S11 TG curve of (a) NaScF₄ and (b) KSc₂F₇ nanocrystals; FT-IR spectrum of KSc₂F₇ nanocrystals (c) before and (d) after thermal treatment.

The TG curve suggests that the weight of NaScF₄ nanocrystals is decreased fast around 330 °C (**Fig. S11a**), whereas, KSc₂F₇ nanocrystals is around 310 °C (**Fig. S11b**). The thermal treatment of hydrophobic nanocrystals is conducted at 500 °C under the protection of Ar/H₂ for 1 h. The peaks located at 2922 cm⁻¹, 2852 cm⁻¹, 1548 cm⁻¹ and 1465 cm⁻¹ in FT-IR spectra of KSc₂F₇ nanocrystals before thermal treatment (**Fig. S11c**) indicate that there are also alkyl (2922 cm⁻¹ and 2852 cm⁻¹) and carboxyl (1548 cm⁻¹ and 1465 cm⁻¹) groups on the surface. After thermal treatment, the characteristic peaks (2922 cm⁻¹ and 2852 cm⁻¹) disappear (**Fig. S11d**), indicating that the alkyl and carboxyl groups on the surface are removed.

$^1\text{H-NMR}$ spectra and $^{13}\text{C-NMR}$ spectra of the products

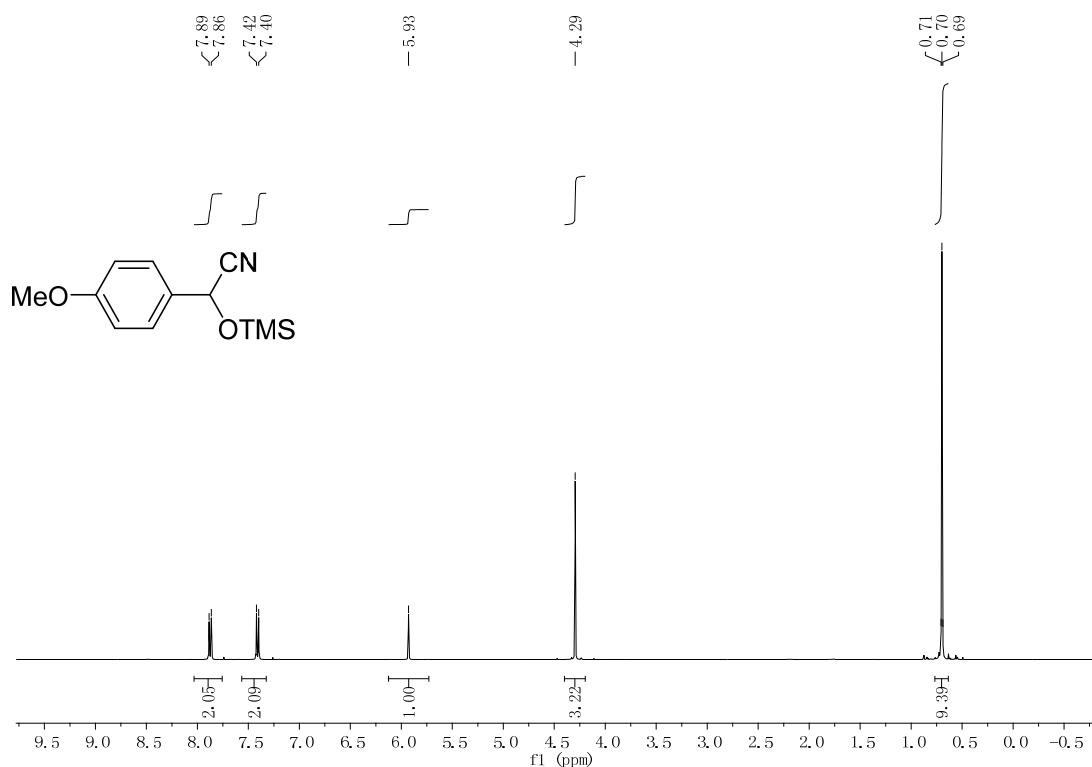


Fig. S12 $^1\text{H-NMR}$ of **1b** in CDCl_3 . Ref: S. T. Kadam and S. Kim, *B. Korean Chem. Soc.*, 2008, **29**, 1320.

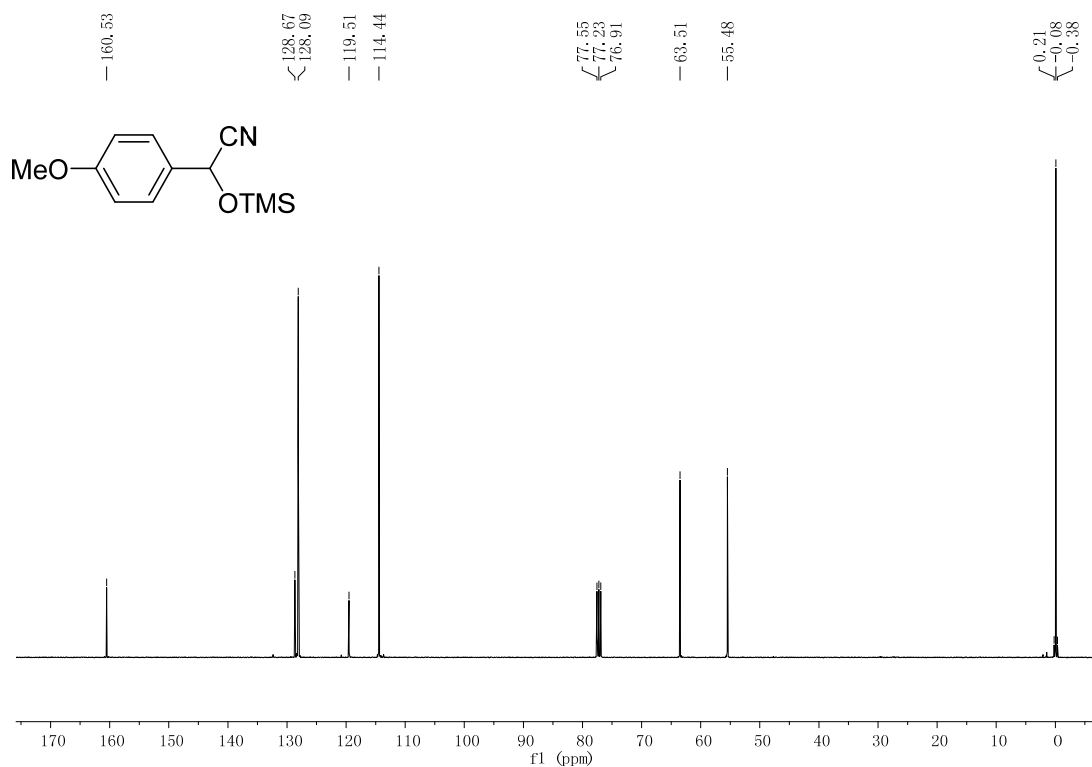


Fig. S13 $^{13}\text{C-NMR}$ of **1b** in CDCl_3 . Ref: A. Baeza, C. Najera, M. de Gracia Retamosa and J. M. Sansano, *Synthesis*, 2005, **16**, 2787.

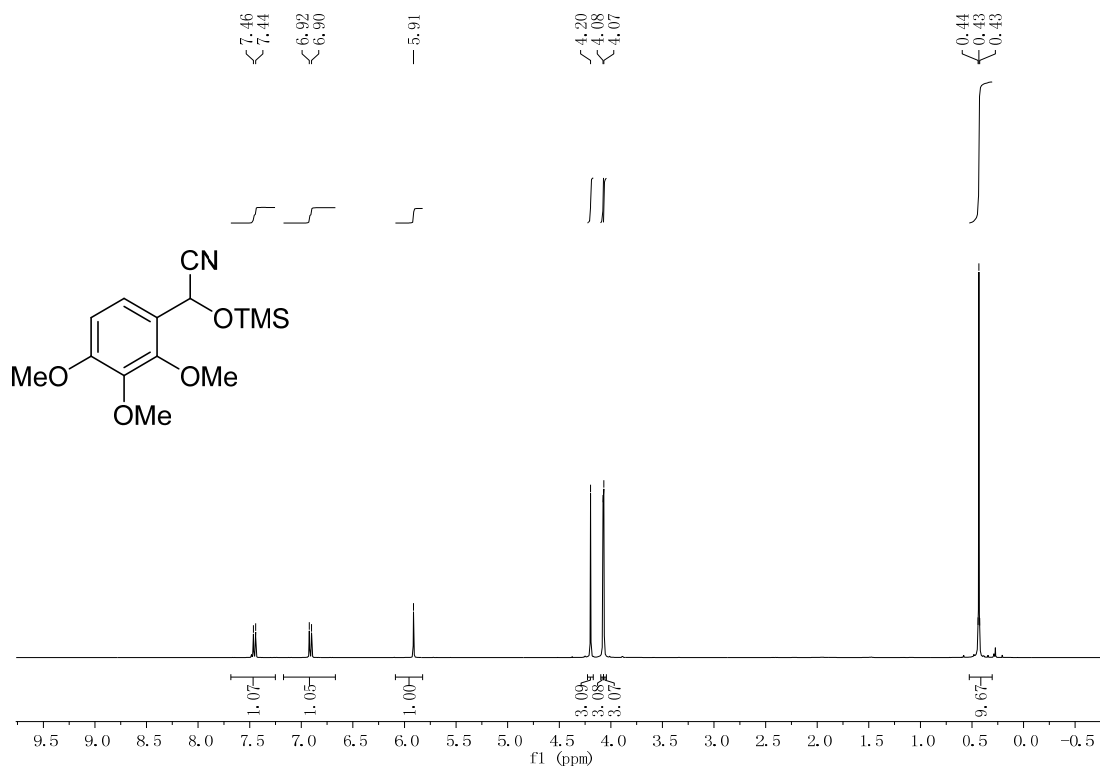


Fig. S14 ¹H-NMR of **2b** in CDCl₃.

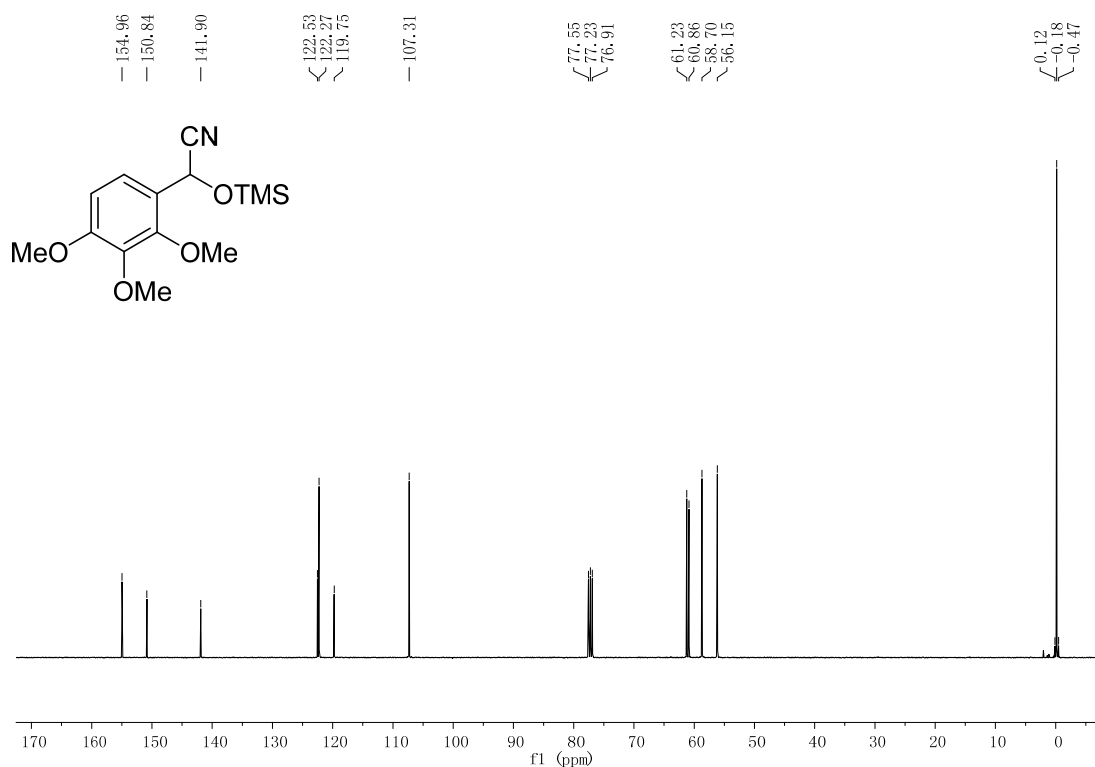


Fig. S15 ¹³C-NMR of **2b** in CDCl₃.

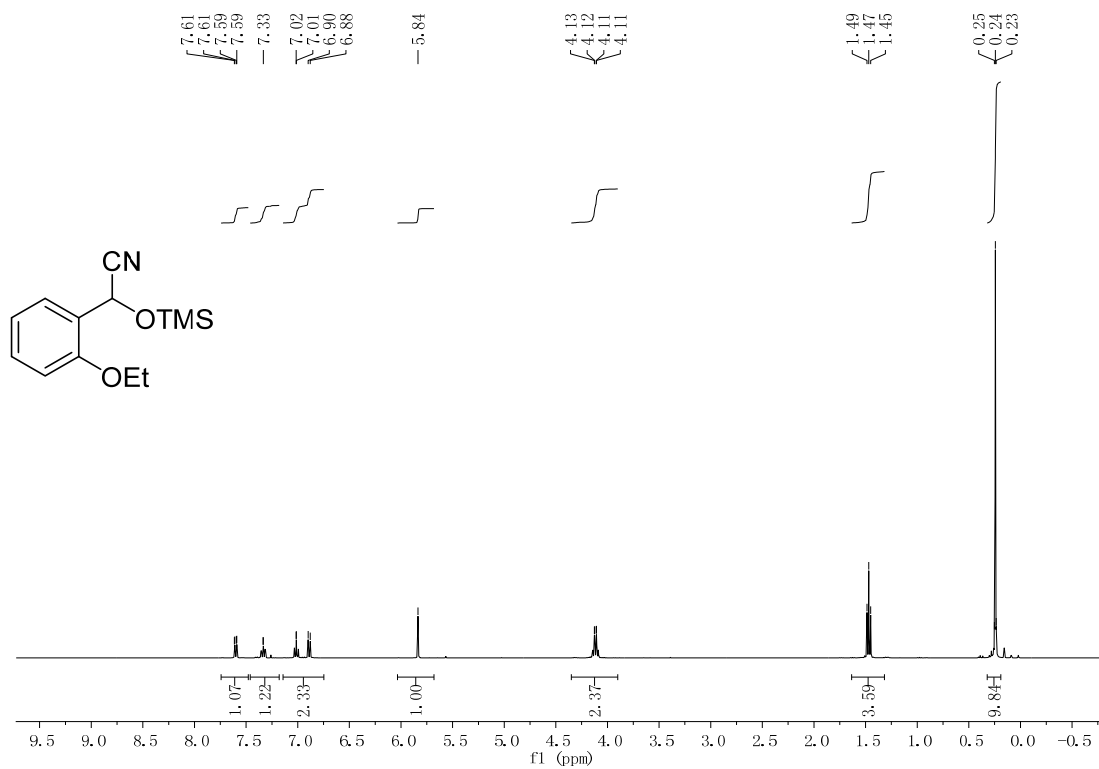


Fig. S16 $^1\text{H-NMR}$ of **3b** in CDCl_3 .

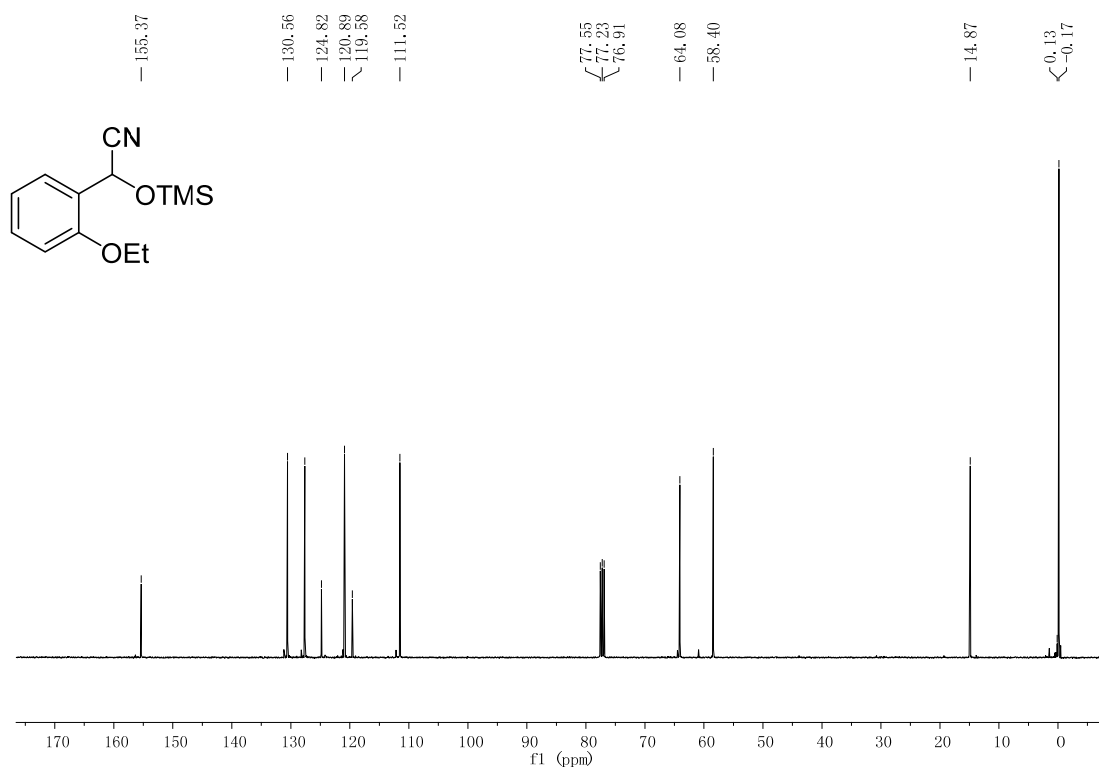


Fig. S17 $^{13}\text{C-NMR}$ of **3b** in CDCl_3 .

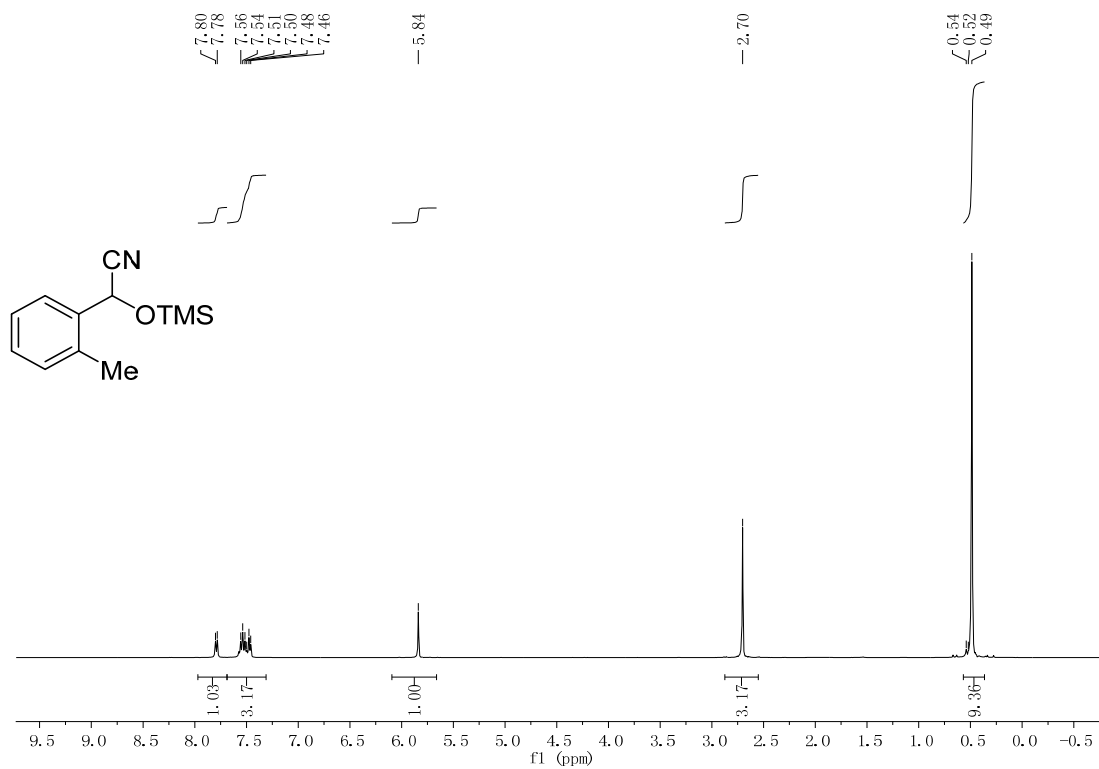


Fig. S18 ¹H-NMR of **4b** in CDCl₃. Ref: H. Härle and J. C. Jochims, *Chemische Berichte*, 1986, **119**, 1400.

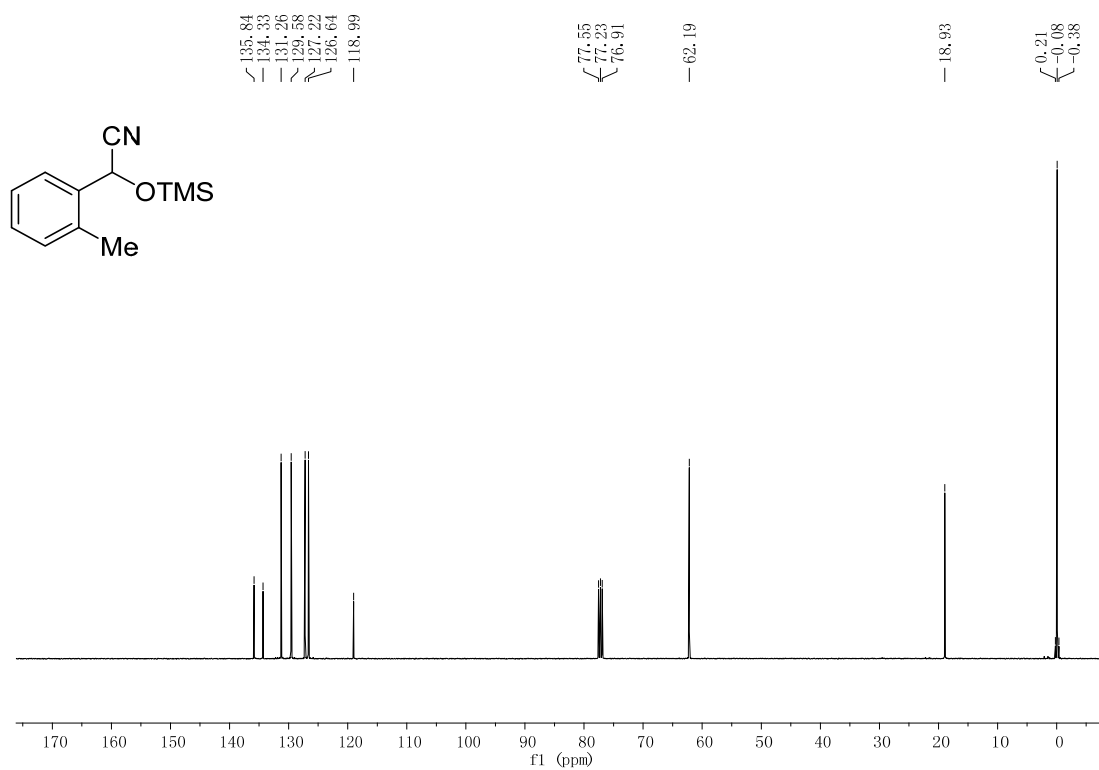


Fig. S19 ¹³C-NMR of **4b** in CDCl₃. Ref: A. Baeza, C. Najera, M. de Gracia Retamosa and J. M. Sansano, *Synthesis*, 2005, **16**, 2787.

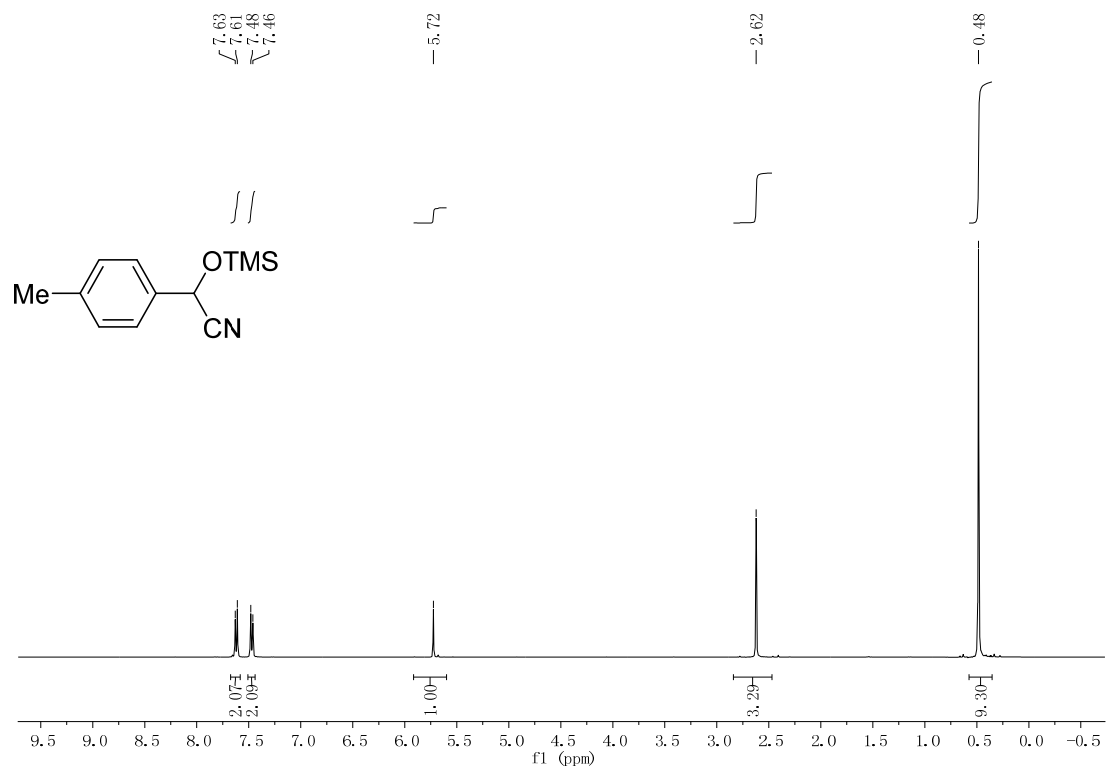


Fig. S20 $^1\text{H-NMR}$ of **5b** in CDCl_3 . Ref: H. Härle and J. C. Jochims, *Chemische Berichte*, 1986, **119**, 1400.

¹³
 $^{13}\text{C-NMR}$ data of **5b** is in Ref: W. P. Neumann and R. Stapel, *Eur. J. Inorg. Chem.*, 1986, **119**, 3432.

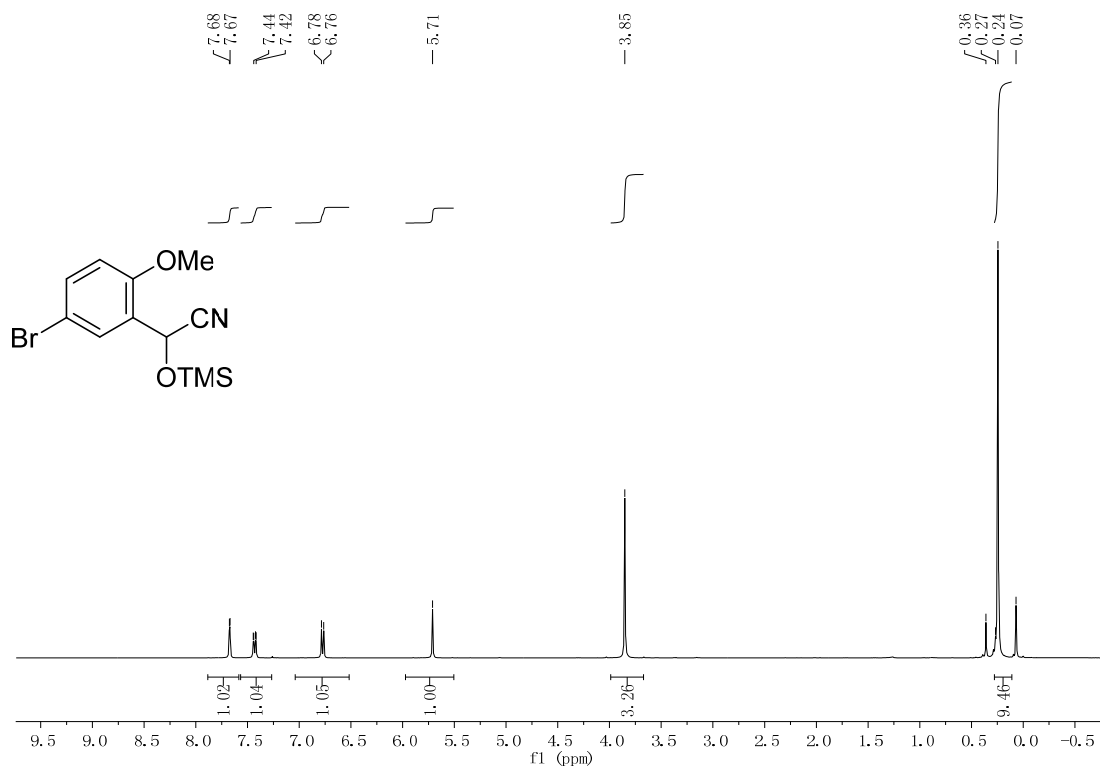


Fig. S21 $^1\text{H-NMR}$ of **6b** in CDCl_3 .

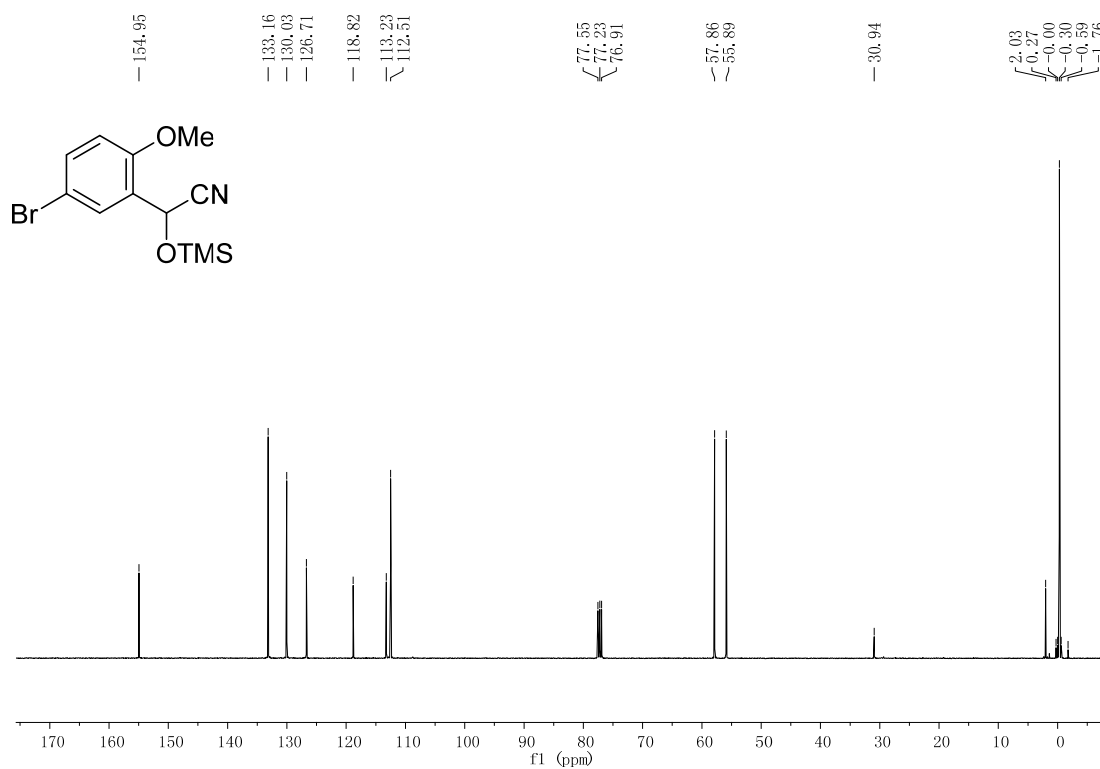


Fig. S22 $^{13}\text{C-NMR}$ of **6b** in CDCl_3 .

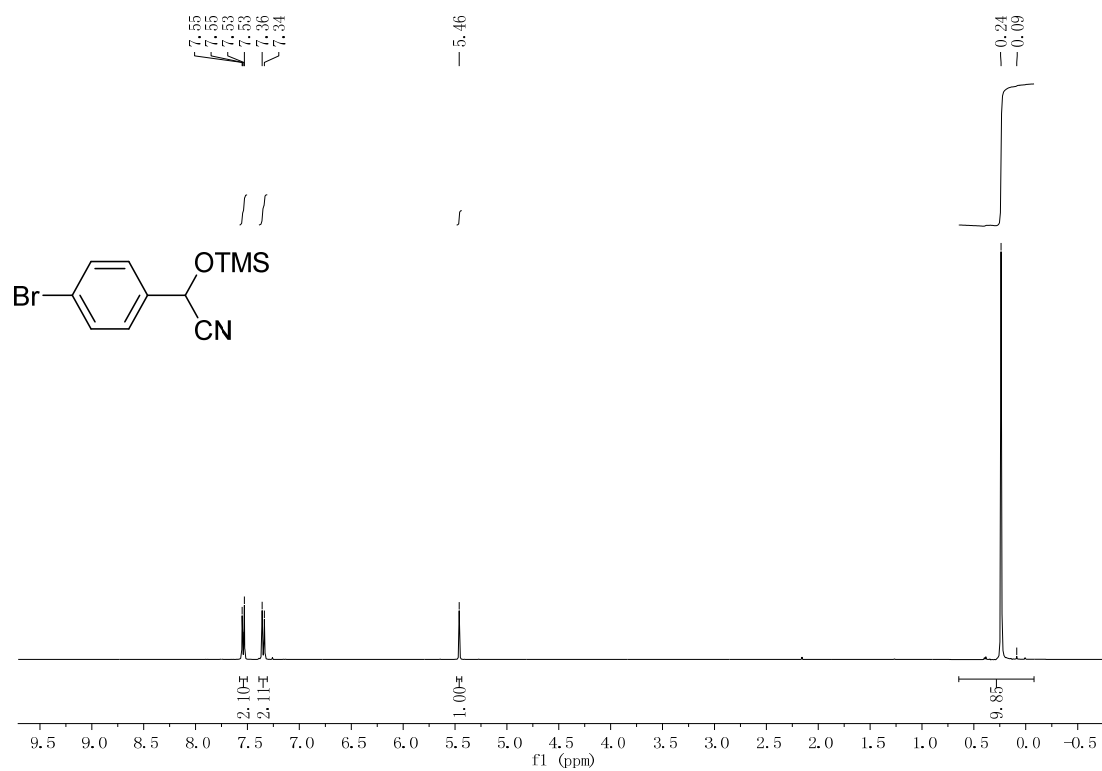


Fig. S23 ¹H-NMR of **7b** in CDCl₃. Ref: L. Mei, K. Yu Ping, L. Xiao Xuan, Y. Hao, H. Ke Liang and J. Ying, *Synthetic Commun.*, 2006, **36**, 2483.

¹³

C-NMR data of **7b** is in Ref: L. Mei, K. Yu Ping, L. Xiao Xuan, Y. Hao, H. Ke Liang and J. Ying, *Synthetic Commun.*, 2006, **36**, 2483.

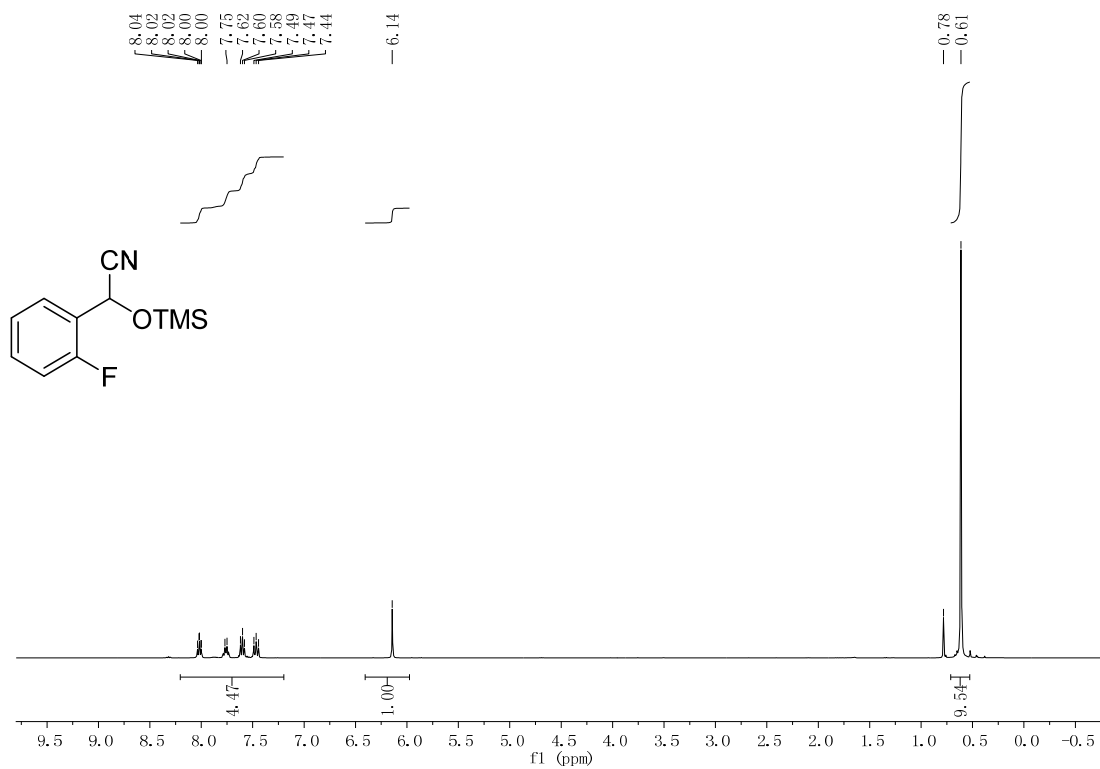


Fig. S24 $^1\text{H-NMR}$ of **8b** in CDCl_3 . Ref: L. Mei, *J. Mol. Catal. A-Chem.*, 2005, **227**, 183.

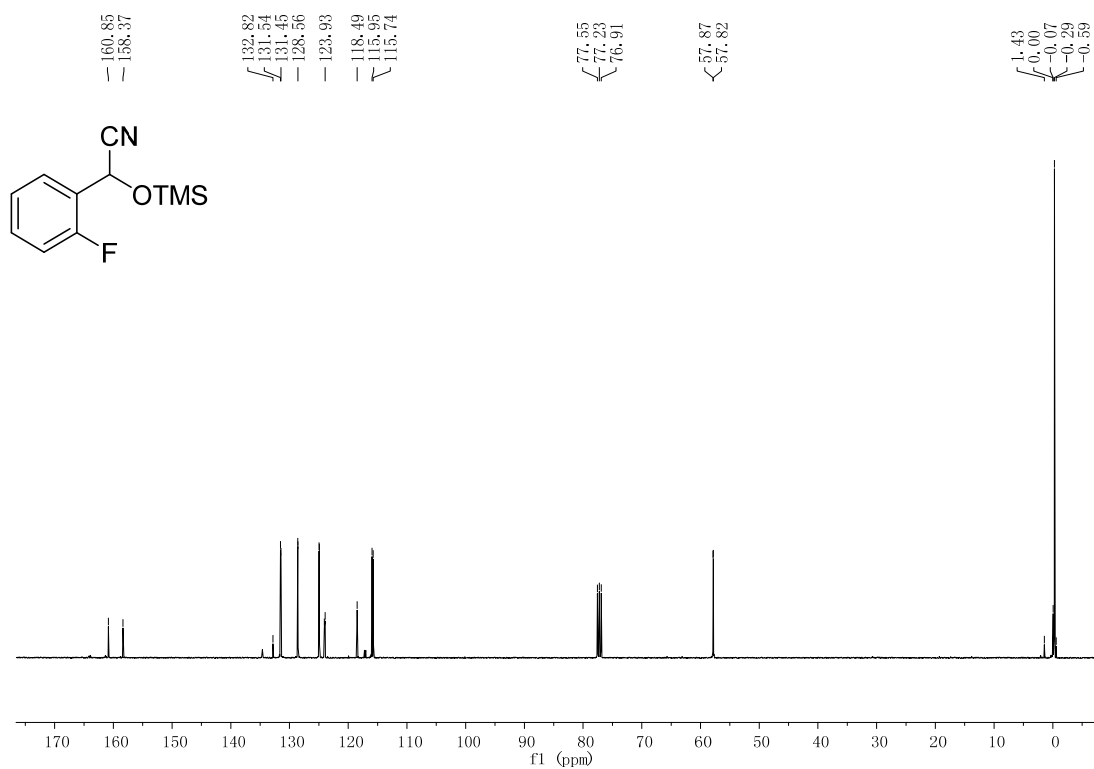


Fig. S25 $^{13}\text{C-NMR}$ of **8b** in CDCl_3 . Ref: L. Mei, *J. Mol. Catal. A-Chem.*, 2005, **227**, 183.

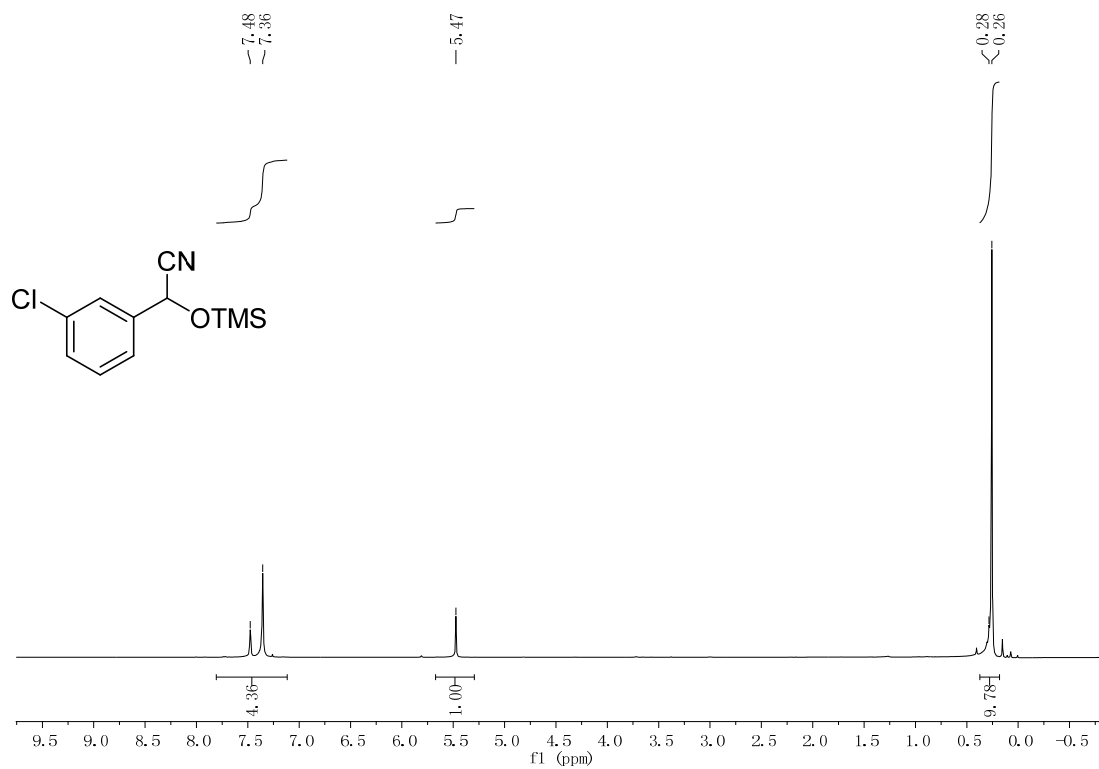


Fig. S26 $^1\text{H-NMR}$ of **9b** in CDCl_3 . Ref: S. C. Georgea and S. Kim, *B. Korean Chem. Soc.*, 2007, **28**, 1167.

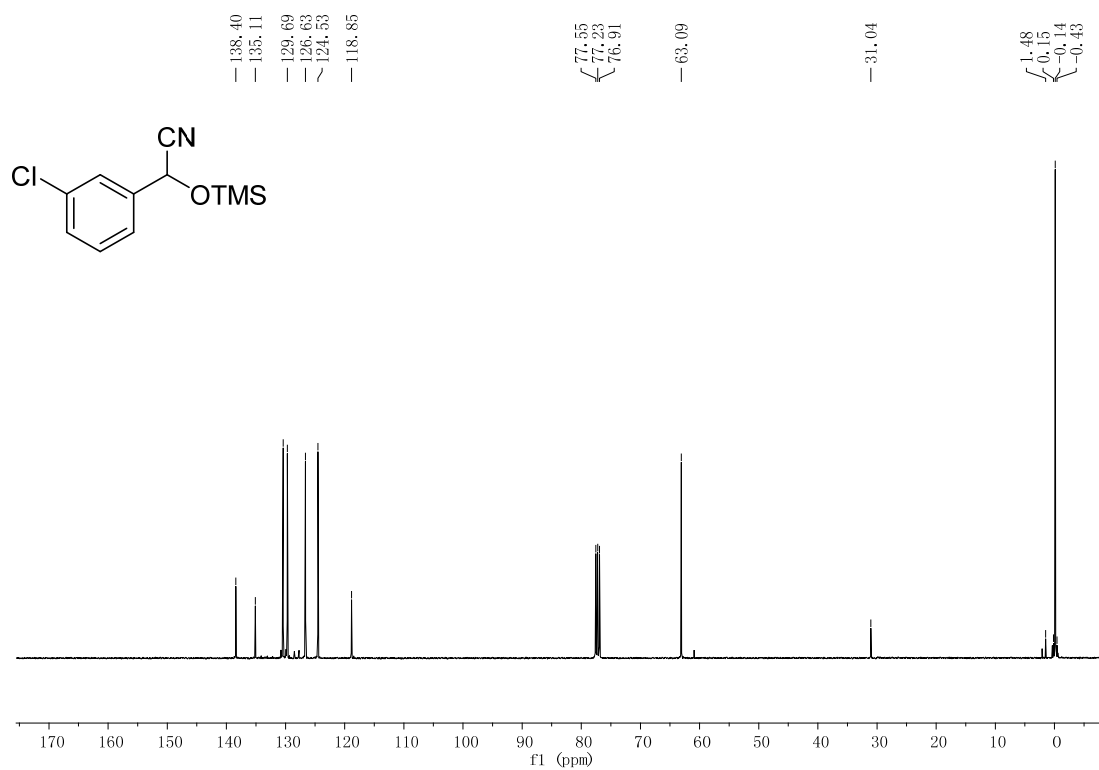


Fig. S27 $^{13}\text{C-NMR}$ of **9b** in CDCl_3 . Ref: S. C. Georgea and S. Kim, *B. Korean Chem. Soc.*, 2007, **28**, 1167.

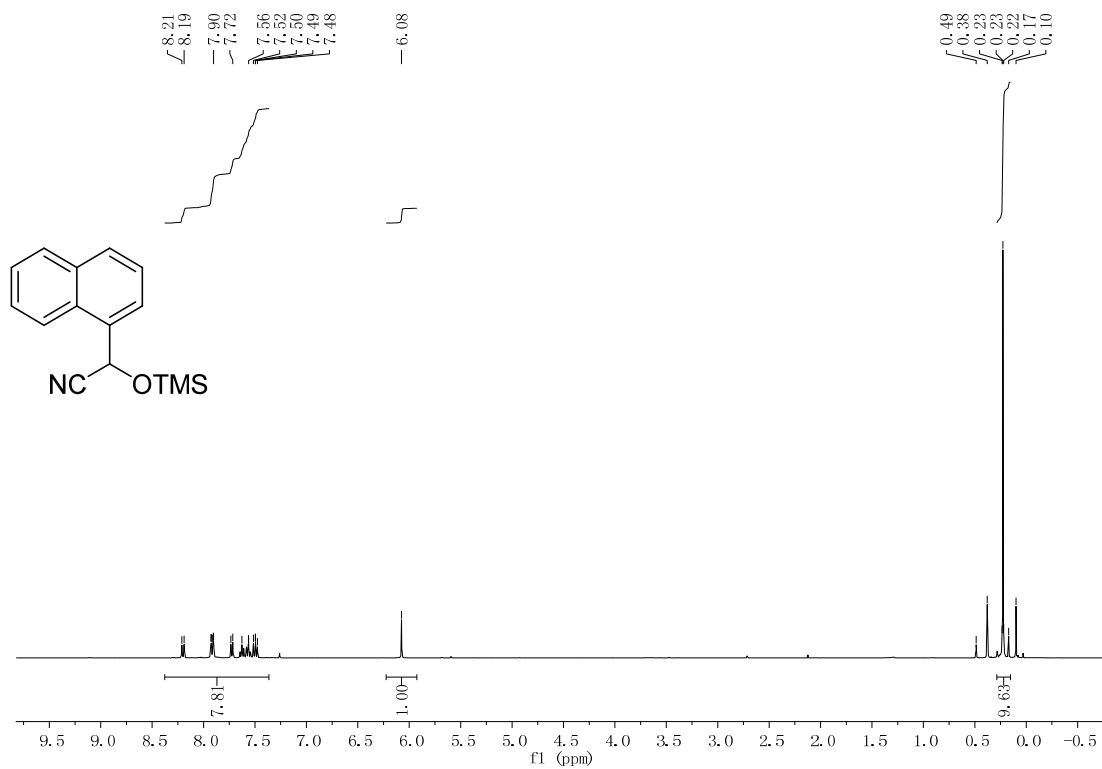


Fig. S28 ¹H-NMR of **10b** in CDCl₃. Ref: L. Mei, *J. Mol. Catal. A-Chem.*, 2005, **227**, 183.

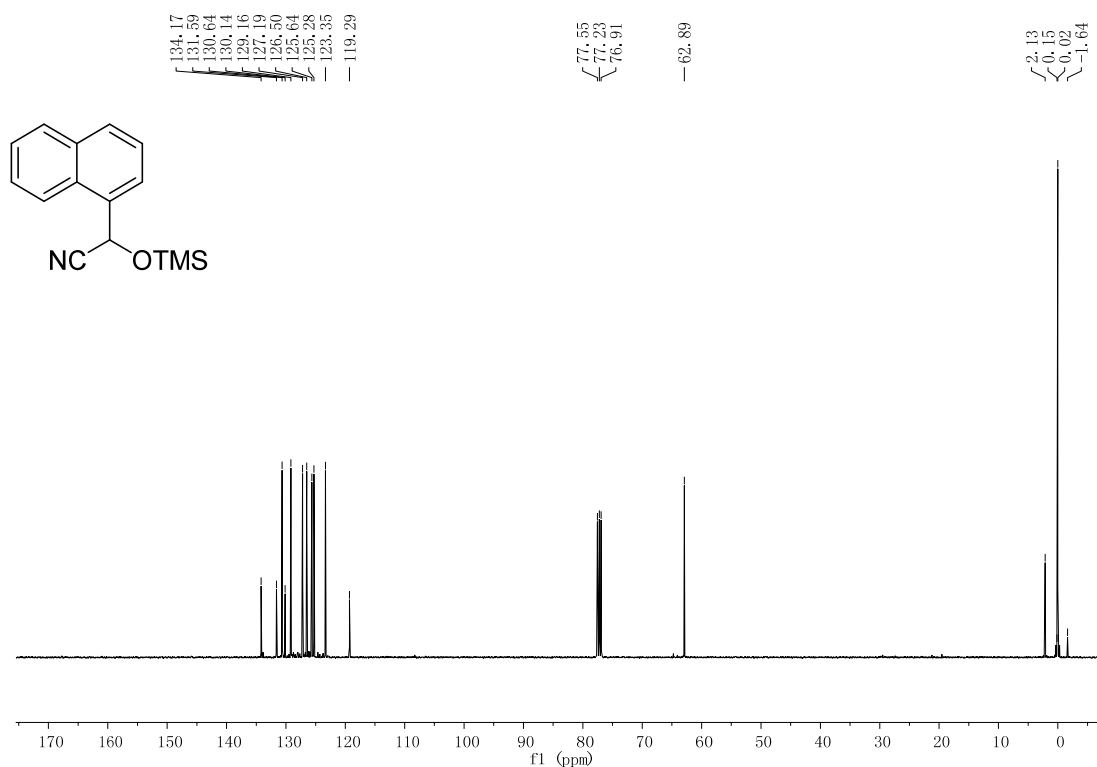


Fig. S29 ¹³C-NMR of **10b** in CDCl₃. Ref: L. Mei, *J. Mol. Catal. A-Chem.*, 2005, **227**, 183.

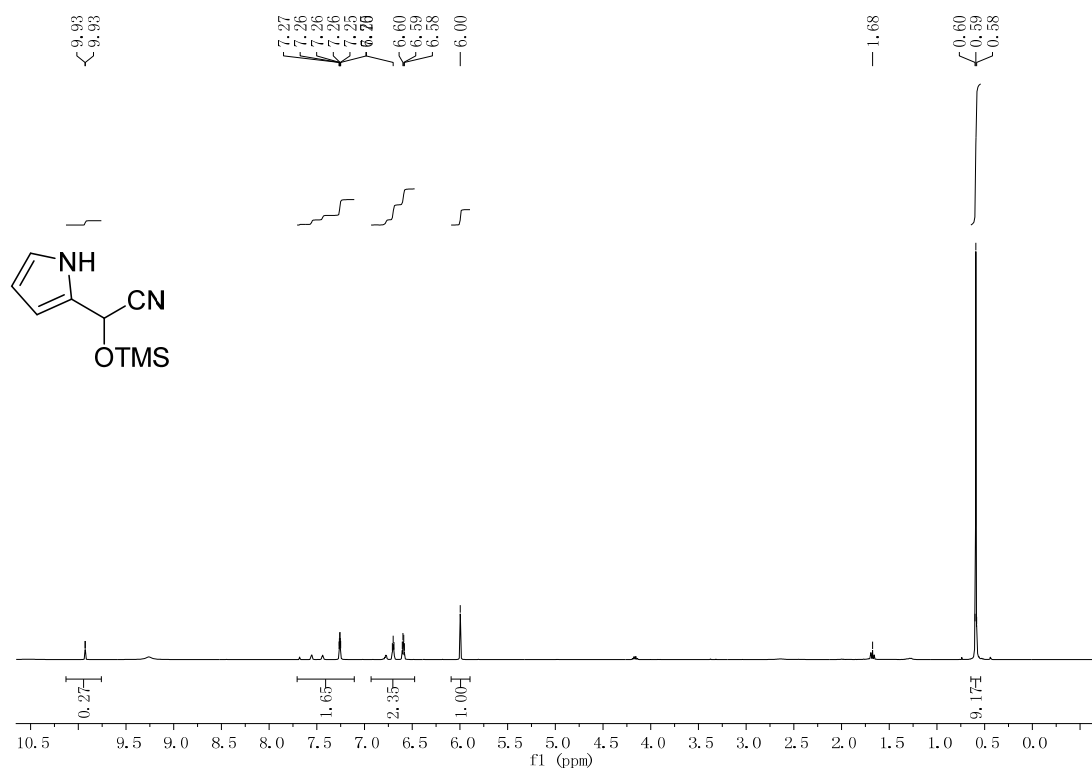


Fig. S30 ¹H-NMR of **11b** in CDCl₃. Ref: S. M. Raders and J. G. Verkade, *Tetrahedron Lett.*, 2009, **50**, 5317.

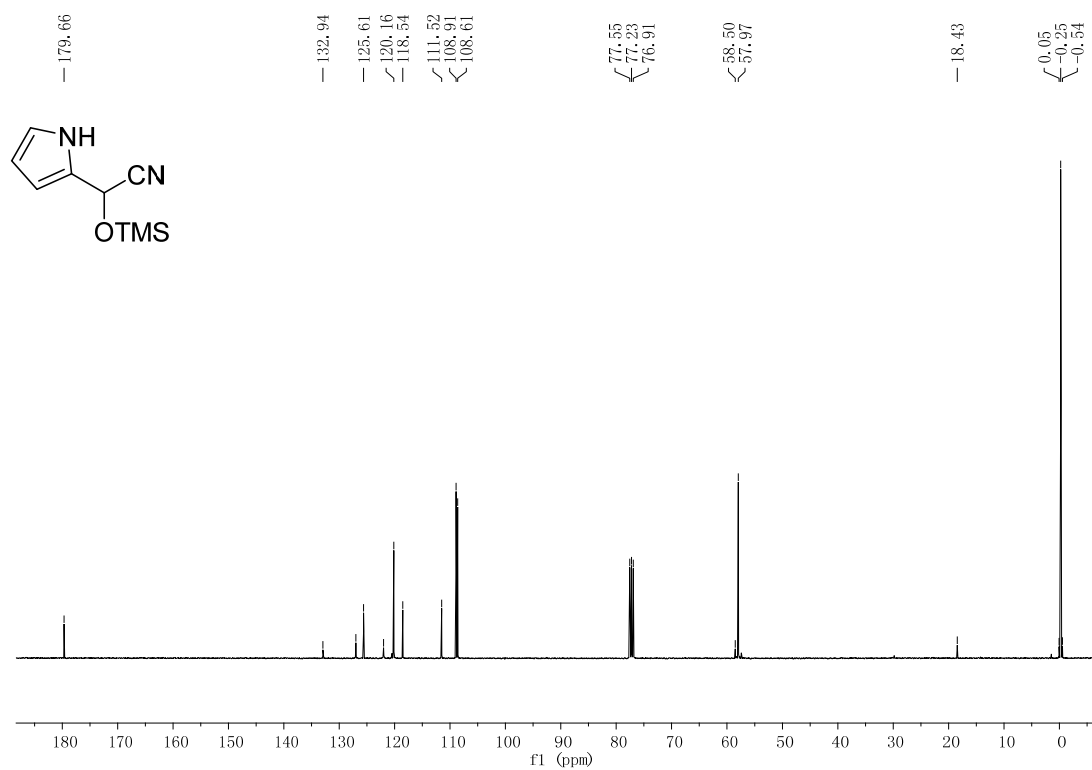


Fig. S31 ¹³C-NMR of **11b** in CDCl₃. Ref: S. M. Raders and J. G. Verkade, *Tetrahedron Lett.*, 2009, **50**, 5317.

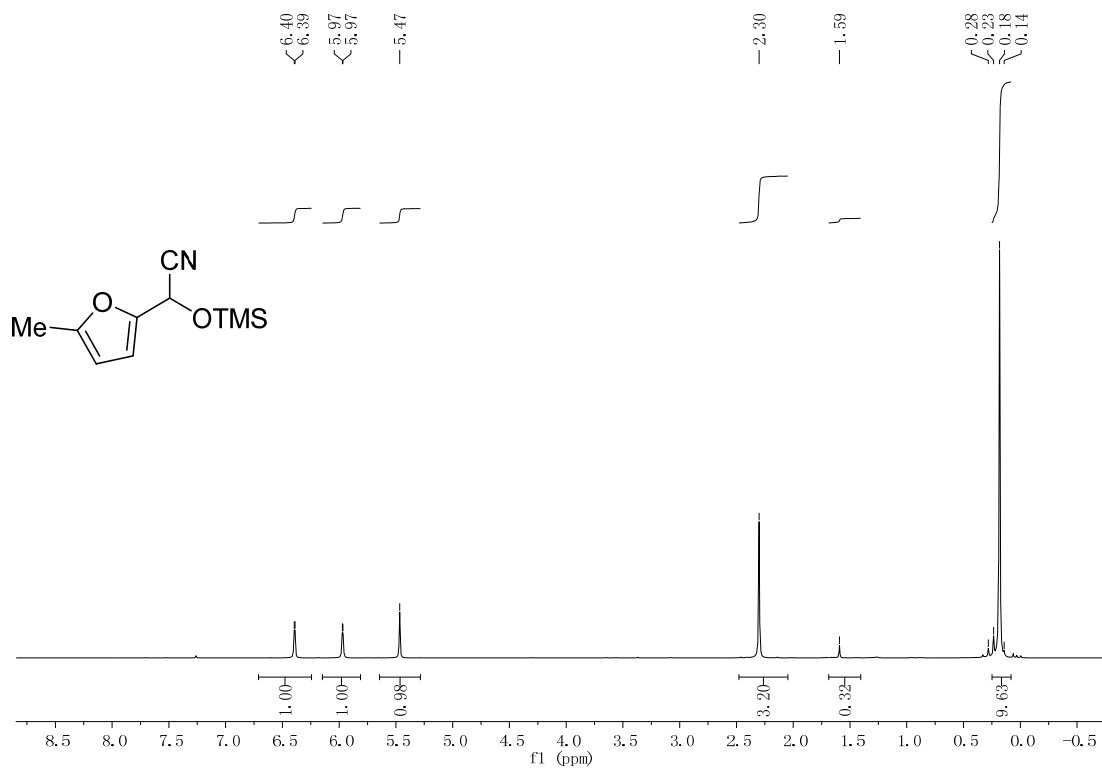


Fig. S32 ¹H-NMR of **12b** in CDCl₃.

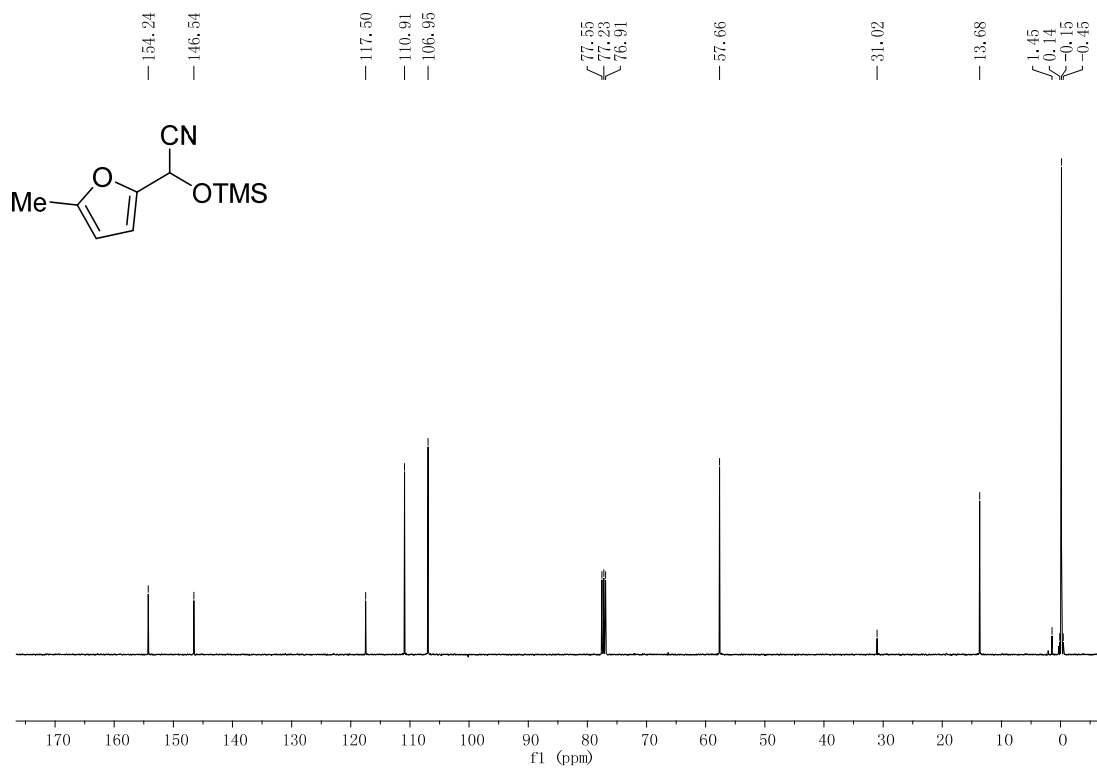


Fig. S33 ¹³C-NMR of **12b** in CDCl₃.

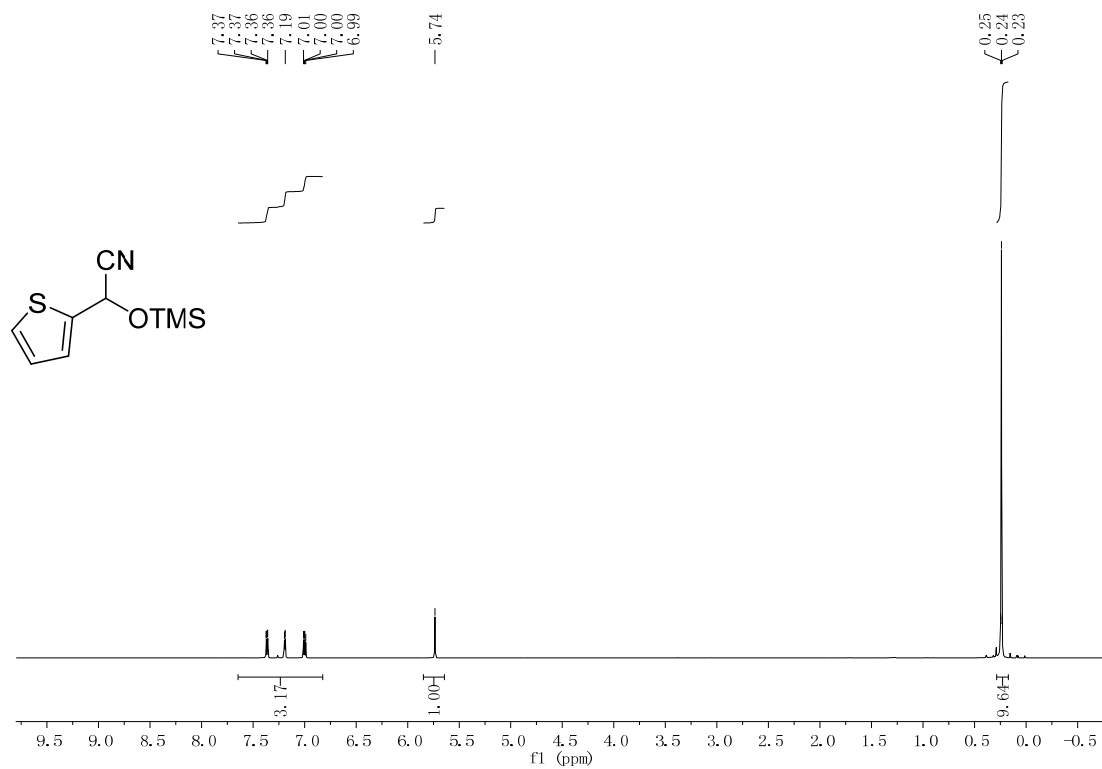


Fig. S34 $^1\text{H-NMR}$ of 13b in CDCl_3 .

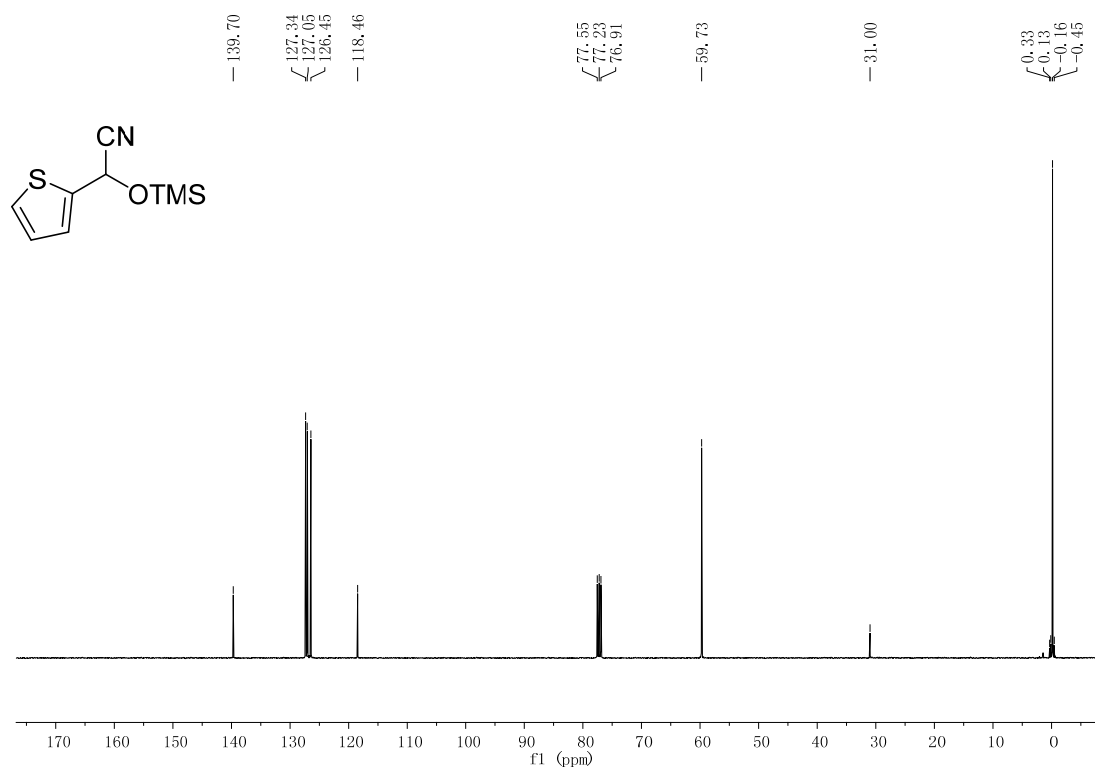


Fig. S35 $^{13}\text{C-NMR}$ of 12b in CDCl_3 .

The comparison of catalytic reactivity

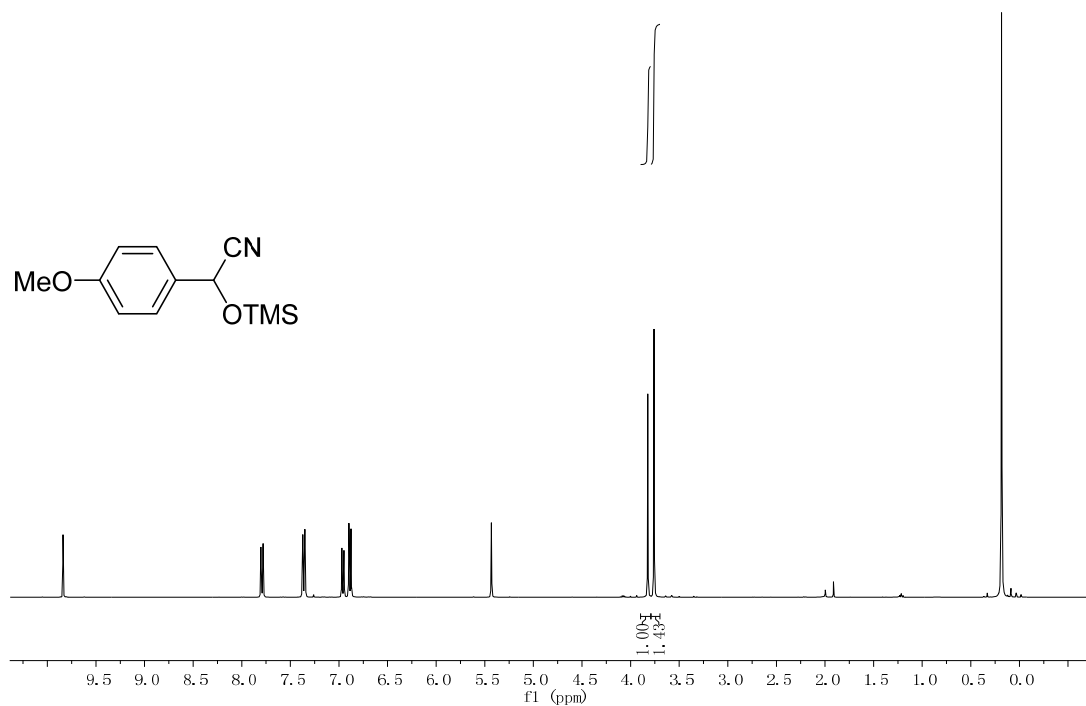


Fig. S36 ¹H-NMR of the conversion of p-anisaldehyde in CDCl₃, the experiment was carried out with 1% NaScF₄ loaded for 24 h, and the conversion is 58.8%.

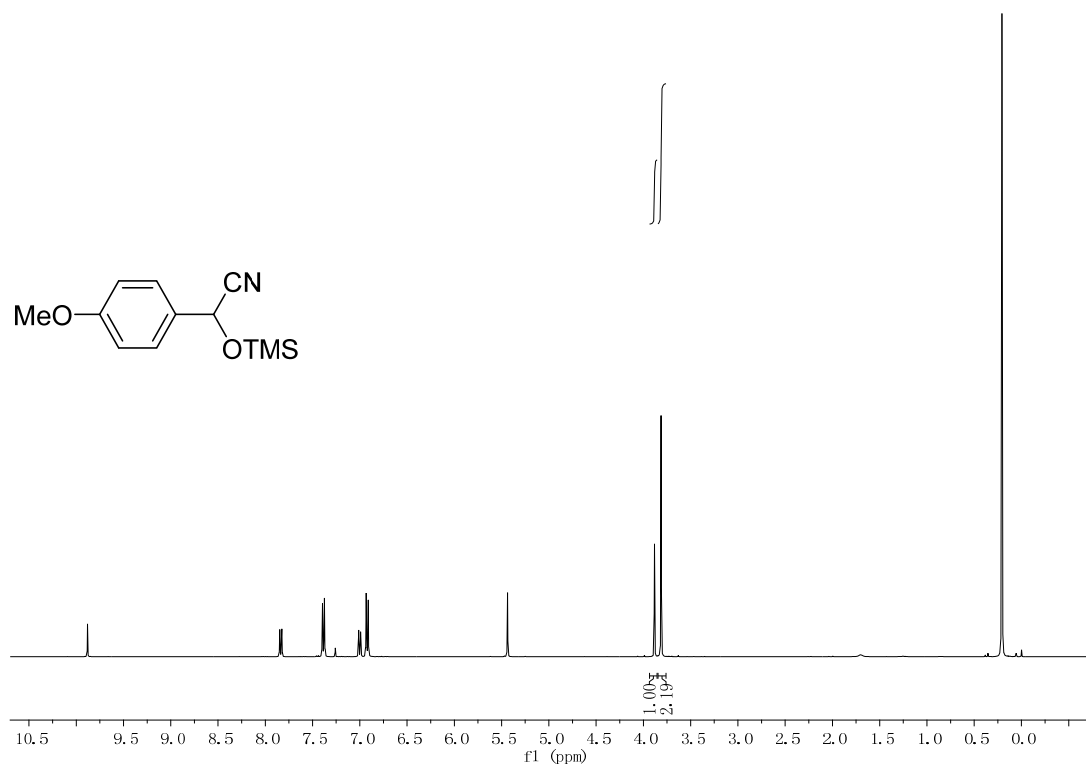


Fig. S37 ¹H-NMR of the conversion of p-anisaldehyde in CDCl₃, the experiment was carried out with 1% KSc₂F₇ loaded for 24 h, and the conversion is 68.6%.

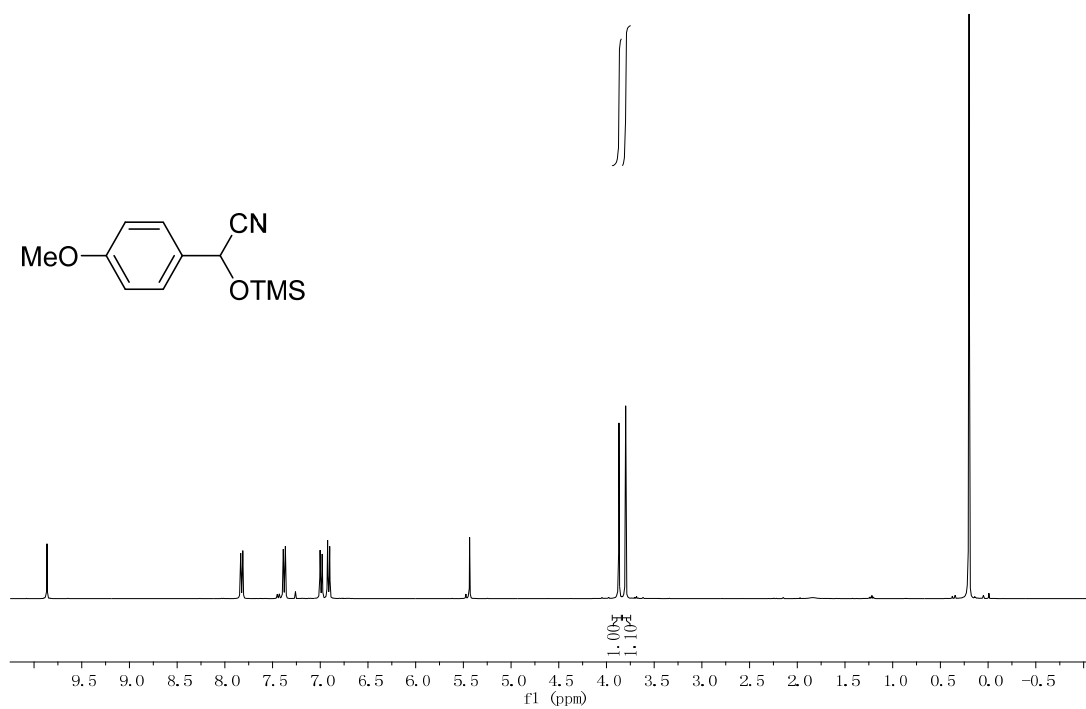


Fig. S38 ¹H-NMR of the conversion of p-anisaldehyde in CDCl₃, the experiment was carried out with 5% NaScF₄ (with the size of ~ 22 nm) loaded for 3 h, and the conversion is 52.4%.

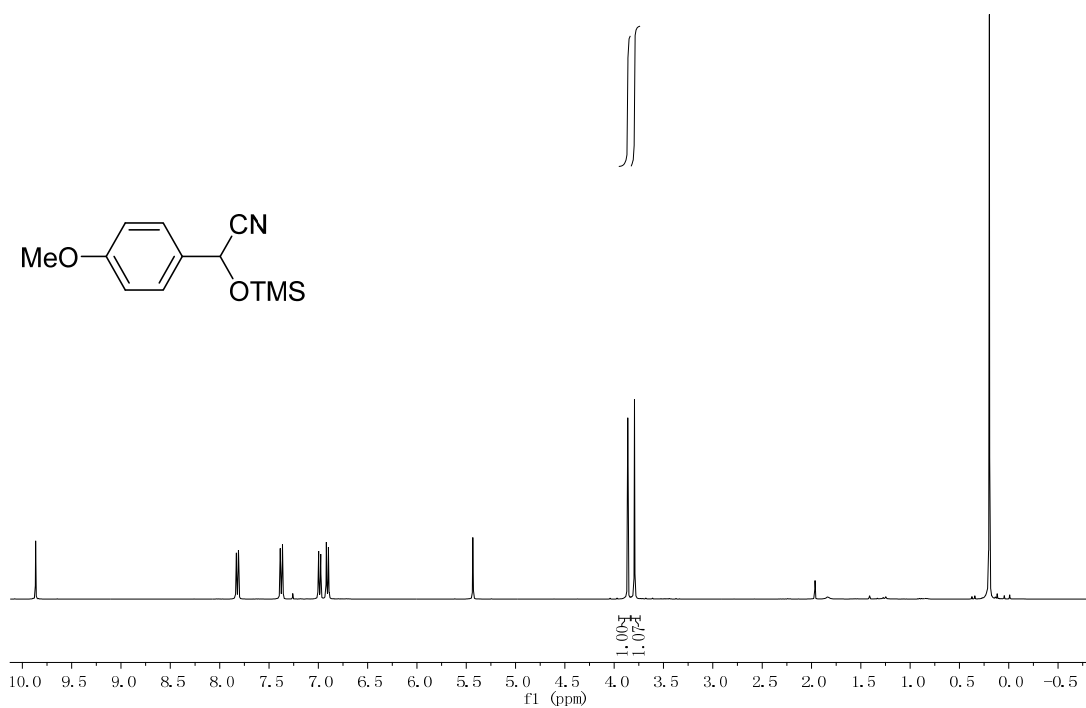


Fig. S39 ¹H-NMR of the conversion of p-anisaldehyde in CDCl₃, the experiment was carried out with 5% NaScF₄ (with the size of ~ 29 nm) loaded for 3 h, and the conversion is 51.7%.

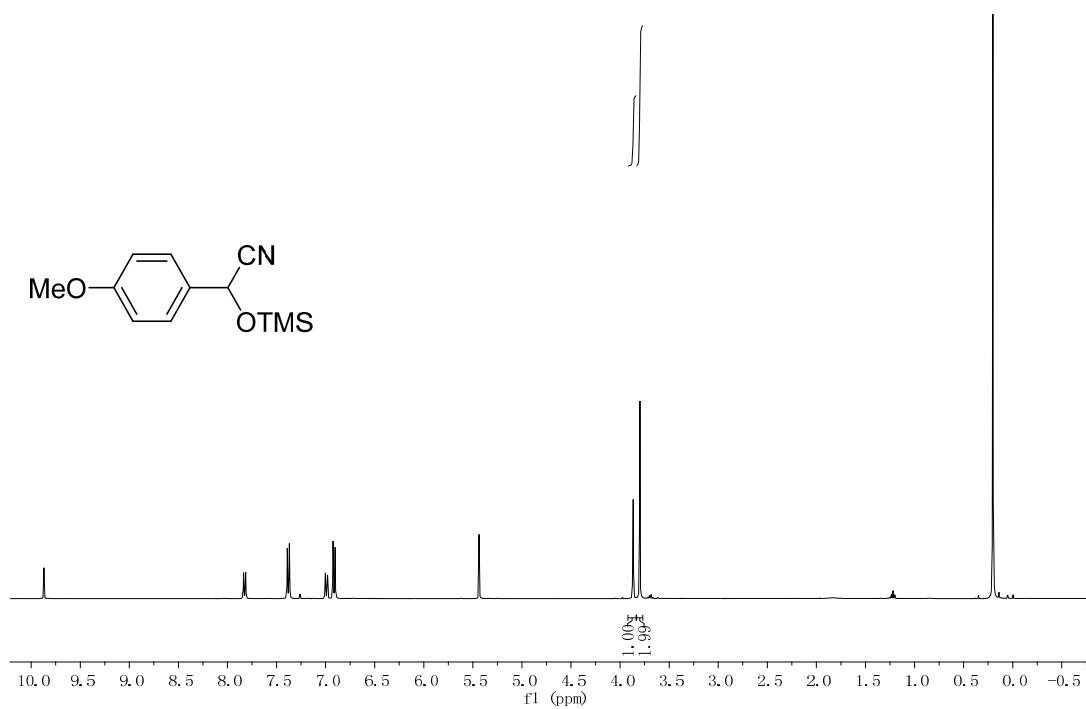


Fig. S40 ¹H-NMR of the conversion of p-anisaldehyde in CDCl₃, the experiment was carried out with 5% NaScF₄ (with the size of ~ 38 nm) loaded for 3 h, and the conversion is 66.6%.

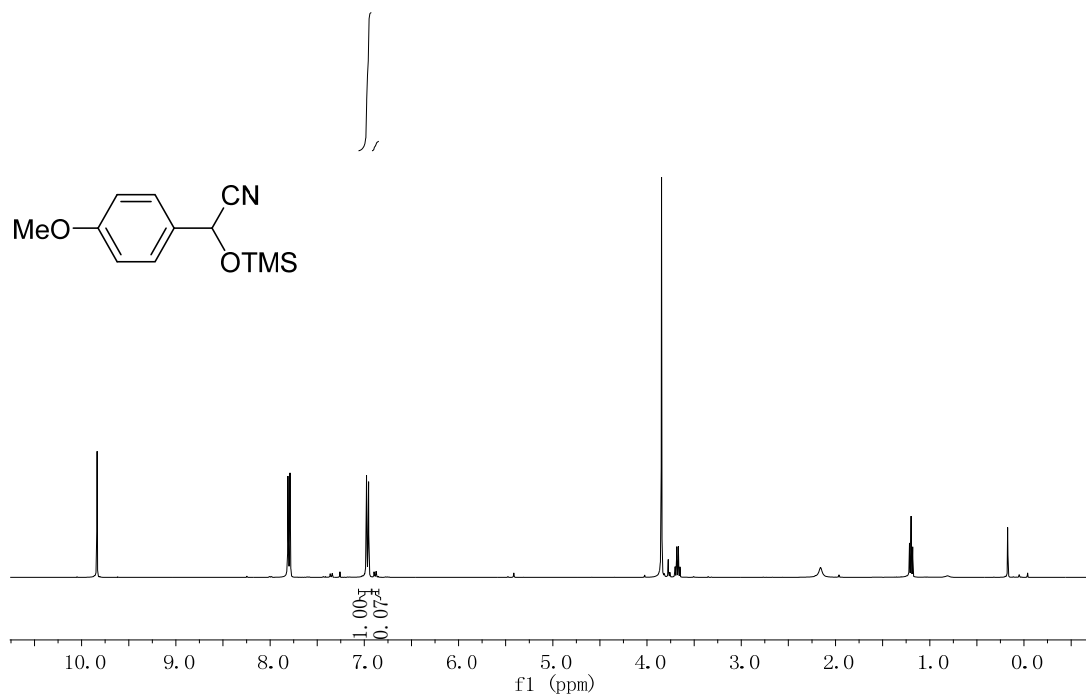


Fig. S41 ¹H-NMR of the conversion of p-anisaldehyde in CDCl₃, the experiment was carried out with 5% bulk NaScF₄ loaded for 10 h, and the conversion is 6.5%.

As shown in $^1\text{H-NMR}$ spectra of **Fig. S36** and **Fig. S37**, the two adjacent peaks are the shifts of H in MeO- group of p-anisaldehyde and **1b**, respectively. The calculated conversion (from the integral of these two peaks) is 58.8% and 68.6% respectively, for 1% loading of NaScF_4 and KSc_2F_7 . In **Fig. S38**, **Fig. S39** and **Fig. S40**, the conversion is 52.4%, 51.7% and 66.6% for 3 h reaction and 5% loading of NaScF_4 nanocrystals with the size of ~ 22 nm, ~ 29 nm and ~ 38 nm, respectively. As for bulk fluorides, the catalytic reactivity is much lower: when experiments carried out with 5% bulk catalysts loaded for 10 h, the conversion of p-anisaldehyde is 6.5% for bulk NaScF_4 and 33.3% for bulk KSc_2F_7 , which are much lower than nanocatalysts, as shown in **Fig. S41** and **Fig. S42**. And the catalytic reactivity of bulk Sc_2O_3 is much lower than fluorides, as shown in **Fig. S43**. The conversions are also summarized in **Table S1**, in which we can easily notice the advantages of nano-sized catalysts, and the similar catalytic reactivity of NaScF_4 nanocrystals with different sizes. It's worth to mention that the bulk Sc_2O_3 has very low catalytic reactivity, so we can ignore the tiny oxidation on the surface of the fluoride nanocrystals.

Table S1 Conversions of aromatic aldehydes substrates when using different catalysts.

Catalyst	Loading (%)	Reaction time (h)	conversion (%)
NaScF_4 (~ 38 nm)	1	24	58.8
KSc_2F_7	1	24	68.6
NaScF_4 (~ 22 nm)	5	3	52.4
NaScF_4 (~ 29 nm)	5	3	51.7
NaScF_4 (~ 38 nm)	5	3	66.6
NaScF_4 (~ 38 nm)	5	10	99
KSc_2F_7	5	10	99
NaScF_4 (bulk)	5	10	6.5
KSc_2F_7 (bulk)	5	10	33.3
Sc_2O_3 (bulk)	5	10	11.5

XRD patterns and TEM images of bulk NaScF₄ and KSc₂F₇

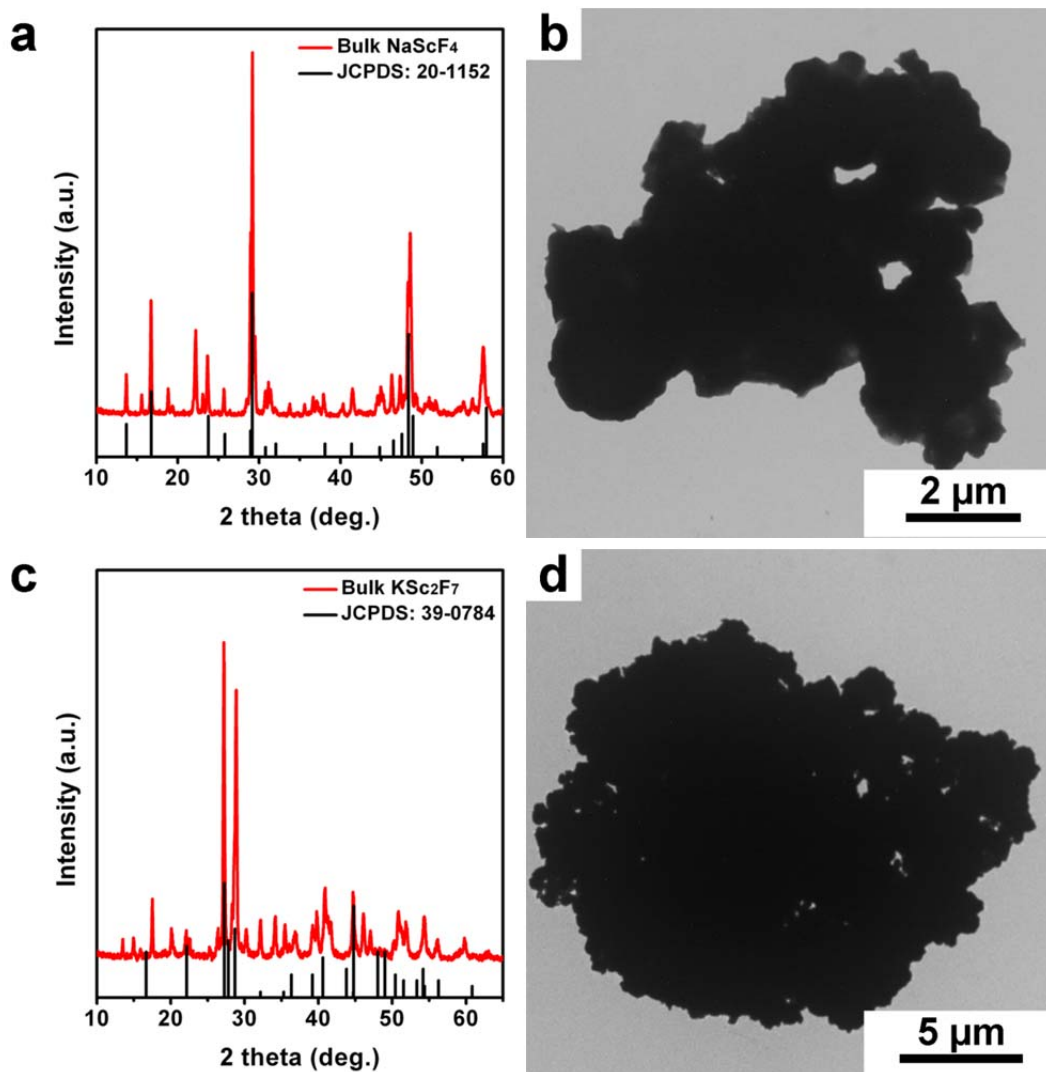


Fig. S44 (a) XRD pattern, (b) TEM image, of bulk NaScF₄; (c) XRD pattern, (d) TEM image, of bulk NaSc₂F₇.

The bulk catalysts (bulk NaScF₄ and KSc₂F₇) are prepared by direct thermal decomposition: 0.3 mmol NaCF₃COO and 0.3 mmol Sc(CF₃COO)₃, or 0.3 mmol KCF₃COO and 0.3 mmol Sc(CF₃COO)₃, are mixed by grinding, and then transferred into tube furnace, without any other reagent addition; the decomposition is conducted at 500 °C in N₂ atmosphere for 1h. After cooling down, the product powder is collected. The obtained bulk NaScF₄ and KSc₂F₇ are of irregular micro-sized bulks, with impurities in XRD patterns, as shown in **Fig. S44**.

BET isotherms of NaScF₄ and KSc₂F₇ nanocatalysts

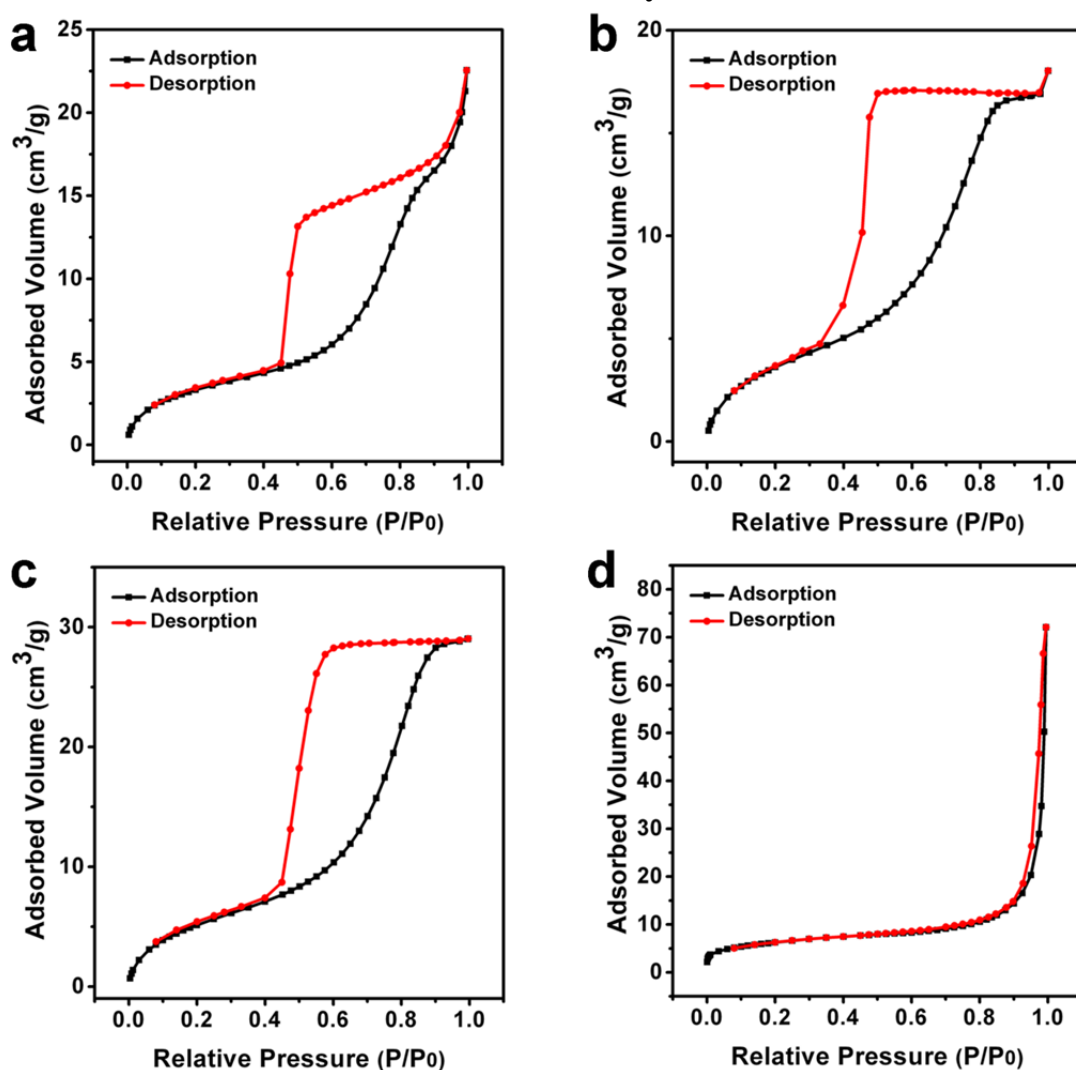


Fig. S45 BET isotherms of NaScF₄ nanocatalysts with the size of (a) ~22 nm, (b) ~29 nm and (c) ~38 nm; (d) BET isotherms of KSc₂F₇ nanocatalysts.

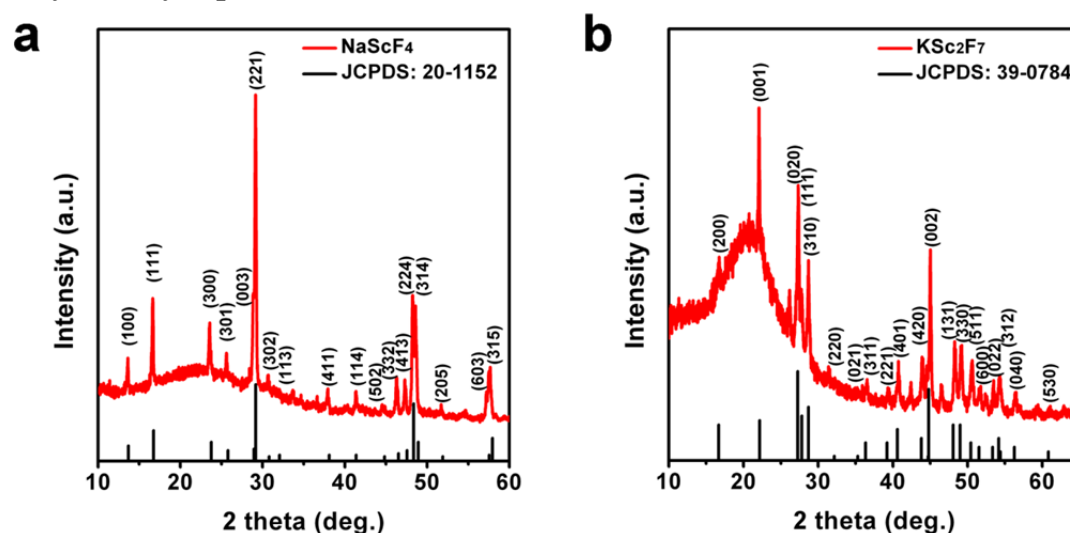
The N₂ adsorption-desorption isotherms of NaScF₄ nanocrystals (**Fig. S45a, b and c**) are of IV type, suggesting the sample is mesoporous and the adsorption can happen inside the catalyst. The N₂ adsorption-desorption isotherm of KSc₂F₇ nanocrystals (**Fig. S45d**) is almost of II type, and the inflection point in low P/P₀ area of the curve represents that the saturated adsorption capacity of monomolecular layer is small, and the convexity of the curve in this area indicates that the adsorption is relatively weak.

Table S2 BET surface area, pore volume and pore size of NaScF₄ and KSc₂F₇ nanocatalysts.

Sample	BET surface area (m ² /g)	Pore volume (cm ³ /g)	Pore size (nm)
NaScF ₄ (~22 nm)	14.5	0.03	7.66
NaScF ₄ (~29 nm)	12.6	0.03	11.1
NaScF ₄ (~38 nm)	20.5	0.04	8.8
KSc ₂ F ₇	21.7	0.11	20.6

The BET analysis results (**Table S2**) show that for NaScF₄, the BET surface area, pore volume and pore size are all smaller than KSc₂F₇, maybe indicating that the property of NaScF₄ is the worse. However, the mesoporous structure of NaScF₄ nanocatalysts is more remarkable than KSc₂F₇ (shown in **Fig. S45**), meaning the adsorption can happen inside the NaScF₄ nanocatalysts more easily, which can improve the catalysis. So finally the catalyzing activities of NaScF₄ and KSc₂F₇ are similar.

Recyclability experiments

**Fig. S46** XRD patterns of (a) NaScF₄ and (b) KSc₂F₇ after catalysis.

XRD patterns of NaScF₄ and KSc₂F₇ nanocrystals after catalysis (**Fig. S46a, b**) indicate that the crystalline structures of them are not changed after reaction.